Stable isotope and calcareous nannofossil assemblage record of the late Paleocene and early Eocene (Cicogna section)

Claudia Agnini[1,2], David J. A. Spofforth[3], Gerald R. Dickens[4,5], Domenico Rio[1], Heiko Pälike[6], Jan Backman[5], Giovanni Muttoni[7,8], and Edoardo Dallanave[9]

[1]Dipartimento di Geoscienze, Università di Padova, Padua, Italy
[2]Istituto di Geoscienze e Georisorse, CNR, Padua, Italy
[3]Robertson, CGG GeoSpec, Llandudno, UK
[4]Department of Earth Sciences, Rice University, Houston, Texas, USA
[5]MARUM, University of Bremen, Bremen, Germany
[6]Department of Geological Sciences, Stockholm University, Stockholm, Sweden
[7]Dipartimento di Scienze della Terra "Ardito Desio", Università Statale di Milano, Milan, Italy
[8]ALP, Alpine Laboratory of Paleomagnetism, Peveragno (CN), Italy
[9]Department of Earth and Environmental Sciences, Ludwig-Maximilians Universität München, Munich, Germany

Correspondence to: Claudia Agnini (claudia.agnini@unipd.it)

Abstract. We present records of stable carbon and oxygen isotopes, $CaCO_3$ content, and changes in calcareous nannofossil assemblages across an 81 m thick section of upper Paleocene–lower Eocene marine sedimentary rocks now exposed along the Cicogna Stream in northeast Italy. The studied stratigraphic section represents sediment accumulation in a bathyal hemipelagic setting from approximately 57.5 to 52.2 Ma, a multi-million-year time interval characterized by perturbations in the global carbon cycle and changes in calcareous nannofossil assemblages. The bulk carbonate $\delta^{13}C$ profile for the Cicogna section, once placed on a common timescale, resembles that at several other locations across the world, and includes both a long-term drop in $\delta^{13}C$ and multiple short-term carbon isotope excursions (CIEs). This precise correlation of widely separated $\delta^{13}C$ records in marine sequences results from temporal changes in the carbon composition of the exogenic carbon cycle. However, diagenesis has likely modified the $\delta^{13}C$ record at Cicogna, an interpretation supported by variations in bulk carbonate $\delta^{18}O$, which do not conform to expectations for a primary signal. The record of $CaCO_3$ content reflects a combination of carbonate dilution and dissolution, as also inferred at other sites. Our detailed documentation and statistical analysis of calcareous nannofossil assemblages show major differences before, during and after the Paleocene–Eocene Thermal Maximum. Other CIEs in our lower Paleogene section do not exhibit such a distinctive change; instead, these events are sometimes characterized by variations restricted to a limited number of taxa and transient shifts in the relative abundance of primary assemblage components. Both long-lasting and short-lived modifications to calcareous nannofossil assemblages preferentially affected nannoliths or holococcoliths such as *Discoaster*, *Fasciculithus*, *Rhomboaster/Tribrachiatus*, *Sphenolithus* and *Zygrhablithus*, which underwent distinct variations in abundance as well as permanent evolutionary changes in terms of appearances and disappearances. By contrast, placoliths such as *Coccolithus* and *Toweius*, which represent the main component of the assemblages, were characterized by a gradual decline in abundance over time. Comparisons of detailed nannofossil assemblage records at the Cicogna section and at ODP Site 1262 support the idea that variations in the relative and absolute abundances, even some minor changes, were globally synchronous. An obvious link is through climate forcing and carbon cycling, although the linkages between variations in calcareous nannoplankton, changes in $\delta^{13}C$ records and oceanography will need additional work.

1 Introduction

A remarkable interval of global warming occurred from the middle Paleocene to the early Eocene, between approximately 59 and 51 million years ago (Ma). This inference comes from a variety of proxies (Huber and Caballero, 2011; Hollis et al., 2012), including the stable oxygen isotope (δ^{18}O) composition of benthic foraminifera (Fig. 1). The precise timing of the long-term temperature rise remains somewhat unconstrained, because absolute ages across the early Eocene remain unsolidified. Throughout this work, we assume that the option 1 (WO-1) timescale presented by Westerhold et al. (2008) is correct (Table 1), but acknowledge that an offset of ca. 400 kyr may occur within the time interval of interest (Vandenberghe et al., 2012). Debate also surrounds the magnitude and distribution of the temperature warming. Earth's surface temperatures, at least at high latitudes and in the deep sea, seem to have risen by at least 6 °C from ca. 59 to 51 Ma (Zachos et al., 2008; Bijl et al., 2009; Huber and Caballero, 2011; Hollis et al., 2012). Indeed, the latter date marks the acme of the Early Eocene Climatic Optimum (EECO), the warmest sustained time interval of the Cenozoic (Zachos et al., 2008; Cramer et al., 2009; Hollis et al., 2012). Such a rise in temperature is not obvious at low latitudes with current data (Pearson et al., 2007; Huber and Caballero, 2011).

Somehow related to long-term global warming were a series of major perturbations in the global carbon cycle, as clearly indicated by stable carbon isotope (δ^{13}C) records in benthic foraminifera (Fig. 1) and bulk carbonate in numerous marine sediment sequences (Shackleton, 1986; Corfield, 1994; Cramer et al., 2003; Zachos et al., 2008, 2010; Westerhold et al., 2011; Slotnick et al., 2012). An overall increase in δ^{13}C occurred through most of the Paleocene, which climaxed in a Cenozoic high at ca. 57.5 Ma (Westerhold et al., 2011), commonly referred to as the Paleocene carbon isotope maximum (PCIM). From this time, δ^{13}C generally decreased to ca. 52.5 Ma. However, when examined at higher temporal resolution, multiple δ^{13}C records show several short-term (< 200 kyr) negative carbon isotope excursions (CIEs; Cramer et al., 2003; Lourens et al., 2005; Nicolo et al., 2007; Agnini et al., 2009; Zachos et al., 2010; Slotnick et al., 2012). Some of these CIEs clearly coincided with rapid warming (above references). The most prominent and most widely documented example of these "hyperthermals" was the Paleocene–Eocene Thermal Maximum (PETM) at ca. 55.5 Ma, but other apparently similar events occurred at ca. 53.7 Ma (H1 or Eocene Thermal Maximum 2, ETM-2), and at ca. 52.5 Ma (K/X, sometimes called ETM-3).

The early Paleogene in general, and the hyperthermals in particular, has attracted considerable geoscience research. On one level, this is because these time intervals represent a range of possible past analogues for understanding the effects of global warming and massive carbon emissions (see Keeling and Whorf, 2004; Zachos et al., 2008). On another level,

this is because the long-term and short-term temperature and carbon cycle perturbations provide new perspectives for how systems on Earth's surface operate. The PCIM probably represents a tremendous storage of ^{13}C-depleted carbon somewhere on Earth's shallow surface (Shackleton, 1986; Kurtz et al., 2003; Komar et al., 2013). In turn, the CIEs probably signify rapid and large inputs of ^{13}C-depleted carbon into the ocean and atmosphere (Dickens et al., 1997; Lourens et al., 2005; Zeebe et al., 2009). The middle Paleocene through early Eocene shows us that Earth's climate and carbon reservoirs were extremely dynamic during past times of global warmth. However, the composition and whereabouts of large quantities of transferable ^{13}C-depleted carbon (e.g., seafloor methane, peat, permafrost) remain uncertain (above references). Indeed, it is not clear if and how the long-term and short-term carbon cycle perturbations were related to one another, or to Earth surface temperatures.

The above context presents a series of basic questions to the geoscience community. Two of these are the focus of our study. (1) What is the correct template for understanding carbon cycling during the early Paleogene? Major changes in fluxes of ^{13}C-depleted carbon to the ocean or atmosphere should give predictable and coherent signals in the δ^{13}C of carbon-bearing phases across Earth, as well as the distribution of carbonate dissolution on the seafloor. This is not yet established. For example, several recently published δ^{13}C records (Kirtland-Turner et al., 2014; Slotnick et al., 2015a; Payros et al., 2015) do not precisely correlate with those at other locations (Cramer et al., 2003; Zachos et al., 2010; Slotnick et al., 2012, 2015b), at least with available stratigraphy. (2) How did marine calcifying organisms respond to major early Paleogene perturbations in temperature and carbon cycling, both in terms of evolution and preservation? The prominent changes in temperature and carbon fluxes almost assuredly caused large variations in seawater pH and carbonate ion concentration (CO_3^{2-}; Dickens et al., 1997; Zachos et al., 2005; Kump et al., 2009; Zeebe et al., 2009; Leon-Rodriguez and Dickens, 2010; Hönisch et al., 2012; Pälike et al., 2012), although the response should depend on location and carbon fluxes involved (Dickens, 2000; Zeebe and Westbroek, 2003; Komar et al., 2013). Such changes might also affect the ability of living organisms to calcify (Riebesell et al., 2000, 2008; Kleypas et al., 2006; Iglesias-Rodriguez et al., 2008; Stillman and Paganini, 2015), which might impact the fossil record (Agnini et al., 2006; Raffi and De Bernardi, 2008; Erba et al., 2010; Hönisch et al., 2012).

In regards to both questions, calcareous nannoplankton are an obvious group of organisms to focus on. This is because they are a main component of open-ocean primary production (Milliman, 1993; Winter et al., 1994; Rost and Riebesell, 2004), because they dominate the output of carbonate in the ocean (Ziveri et al., 1999; Hay, 2004), and because they exhibit marked changes in species composition from the middle Paleocene through the early Eocene (Romein, 1979; Aubry, 1998; Bown et al., 2004; Gibbs et al., 2012).

Table 1. Stratigraphic heights and ages of polarity chron boundaries, key calcareous nannofossil datums, and CIEs at the Cicogna section and ODP Site 1262.

Event		Nanno zones			Cicogna section		DAMR09I	W01	CK95	GTS04	GTS12	Site 1262		AG07+/this study	W01	CK95	GTS04	GTS12
		NP[a]	CP[b]	CN[c]	Height (m)	Err. (m)	Chron notation	Age (Ma)	Age (Ma)	Age (Ma)	Age (Ma)	Depth (mcd)	Err. (m)	Chron notation	Age (Ma)	Age (Ma)	Age (Ma)	Age (Ma)
	C23r base				77.94		0.000	52.364	52.364	52.648	52.620	105.88		0.000	52.364	52.364	52.648	52.620
	K-X base				72.20	0.10	C24n.1n 0.786	52.57	52.60	52.93	52.98	–	–	–	–	–	–	–
B	Discoaster lodoensis	NP12	CP10		71.10	0.10	C24n.1n 0.936	52.61	52.64	52.98	53.05	107.67	0.18	C24n.1n 0.777	52.57	52.60	52.92	52.97
Bc	Chiphragmalithus spp.				71.10	0.10	C24n.1n 0.936	52.61	52.64	52.98	53.05	107.67	0.18	C24n.1n 0.777	52.57	52.60	52.92	52.97
	C24n.1n base				70.64		0.000	52.630	52.663	53.004	53.074	108.19		0.000	52.630	52.663	53.004	53.074
	C24n.1r base				68.80		0.000	–	52.757	53.116	53.199	–		0.000	–	52.757	53.116	53.199
	C24n.2n base				68.21		0.000	–	52.801	53.167	53.274	–		0.000	–	52.801	53.167	53.274
B	Chiphragmalithus spp.				66.50	0.50	C24n.2r 0.473	52.82	52.85	53.22	53.34	109.22	0.10	C24n.2r/.1r 0.358	52.77	52.75	53.11	53.20
	J base				65.40	0.10	C24n.2r 0.778	52.94	52.88	53.26	53.38	109.96	0.02	C24n.2r/.1r 0.616	52.88	52.81	53.18	53.28
	C24n.2r base				64.60		0.000	53.030	52.903	53.286	53.416	111.06		0.000	53.03	52.903	53.286	53.416
B	Girgisia gammation				61.20	0.10	C24n.3n 0.526	53.29	53.14	53.56	53.71	113.52	0.11	C24n.3n 0.540	53.30	53.14	53.57	53.72
Br	Discoaster lodoensis				60.40	0.10	C24n.3n 0.650	53.36	53.19	53.63	53.78	113.52	0.11	C24n.3n 0.540	53.30	53.14	53.57	53.72
T	Discoaster multiradiatus				60.20	0.10	C24n.3n 0.681	53.37	53.21	53.64	53.80	113.52	0.11	C24n.3n 0.540	53.30	53.14	53.57	53.72
	I1/I2 base				60.10	0.10	C24n.3n 0.697	53.38	53.21	53.65	53.81	113.66	0.02	C24n.3n 0.570	53.32	53.16	53.58	53.74
	C24n.3n base				58.14	0.10	0.000	53.530	53.347	53.808	53.983	115.61		0.000	53.530	53.347	53.808	53.983
	H1-Elmo/H2 base				53.90	0.10	C24r 0.090	53.81	53.58	54.06	54.26	117.21	0.01	C24r 0.042	53.66	53.46	53.93	57.12
T	Tribrachiatus contortus	NP11	CP9b		52.70	0.10	C24r 0.115	53.89	53.64	54.14	54.34	118.09	0.10	C24r 0.066	53.74	53.52	54.00	57.14
Tc	Discoaster multiradiatus				51.50	0.10	C24r 0.141	53.97	53.71	54.21	54.42	119.38	0.11	C24r 0.100	53.84	53.60	54.09	57.16
B	Sphenolithus radians				51.30	0.10	C24r 0.145	53.98	53.72	54.22	54.43	118.72	0.10	C24r 0.083	53.79	53.56	54.04	57.15
B	Tribrachiatus orthostylus			CNE3	51.30	0.10	C24r 0.145	53.98	53.72	54.22	54.43	120.67	0.10	C24r 0.134	53.95	53.69	54.19	57.18
T	Tribrachiatus bramlettei				48.50	0.50	C24r 0.204	54.17	53.87	54.39	54.62	121.30	0.11	C24r 0.151	54.00	53.73	54.24	57.18
B	Tribrachiatus contortus		CP9a		45.50	0.50	C24r 0.268	54.37	54.03	54.57	54.82	125.50	0.10	C24r 0.263	54.35	54.02	54.56	57.25
B	Discoaster diastypus		CP9a		42.70	0.10	C24r 0.327	54.55	54.18	54.74	55.00	127.45	0.10	C24r 0.314	54.51	54.15	54.71	57.28
B	Tribrachiatus bramlettei	NP10			35.58	0.55	C24r 0.478	55.03	54.57	55.17	55.47	133.34	0.11	C24r 0.471	55.00	54.55	55.15	57.36
T	Fasciculithus spp./F. tympaniformis				34.73	0.13	C24r 0.496	55.08	54.61	55.22	55.53	135.87	0.11	C24r 0.538	55.21	54.72	55.35	57.40
T	Rhomboaster spp.			CNE2	32.52	0.48	C24r 0.543	55.23	54.73	55.36	55.67	139.72	0.01	C24r 0.640	54.98	54.55	55.64	57.46
X	Fasciculithus/Zygrhablithus				31.60	0.10	C24r 0.562	55.29	54.78	55.41	55.74	139.80	0.02	C24r 0.643	54.99	54.64	55.64	57.46
Br	Tribrachiatus bramlettei				29.43	0.18	C24r 0.608	55.43	54.90	55.55	55.88	139.99	0.02	C24r 0.648	55.56	55.00	55.66	57.46
B	Discoaster araneus				28.95	0.05	C24r 0.618	55.47	54.93	55.57	55.91	–		C24r	–	–	–	–
B	Rhomboaster spp.	NP9b	CP8b		28.88	0.03	C24r 0.620	55.47	54.93	55.58	55.92	140.02	0.01	C24r 0.648	55.56	55.01	55.66	57.46
	PETM				28.73	0.03	C24r 0.623	55.48	54.94	55.59	55.93	140.13	0.02	C24r 0.652	55.57	55.01	55.67	57.46
	P/E boundary (extrapolated)				28.73	0.03	C24r 0.623	55.48	54.94	55.59	55.93	140.13	0.02	C24r 0.652	55.57	55.01	55.67	57.46
decrease	Fasciculithus spp.				28.73	0.03	C24r 0.623	55.48	54.94	55.59	55.93	140.13	0.02	C24r 0.652	55.57	55.01	55.67	57.46
T	F. richardii gr.			CNE1	28.73	0.03	C24r 0.623	55.48	54.94	55.59	55.93	140.13	0.02	C24r 0.652	55.57	55.14	55.67	57.46
	? base				25.00	0.10	C24r 0.702	55.73	55.14	55.81	56.17	142.00	0.02	C24r 0.701	55.72	55.14	55.81	57.49
	D1/D2 base				20.00	0.10	C24r 0.808	56.06	55.41	56.12	56.50	146.17	0.02	C24r 0.812	56.07	55.42	56.13	57.55
	C1/C2 base				12.61	0.10	C24r 0.964	56.55	55.81	56.56	56.99	152.08	0.02	C24r 0.969	56.56	55.82	56.58	57.64
T	Ericsonia robusta				11.2	0.2	C24r 0.994	56.64	55.89	56.65	57.08	153.32	0.10	C25n 0.011	56.67	55.91	56.67	57.11
	C24r base				10.93		0.000	56.660	55.904	56.665	57.101	153.25		0.000	56.660	55.904	56.665	57.101
Bc	F. alanii				10.51	0.49	C25n 0.060	56.69	55.93	56.70	57.13	152.77	0.02	C24r 0.987	56.62	55.87	56.63	57.65
B	Discoaster multiradiatus	NP9a			9.90	0.10	C25n 0.147	56.74	55.98	56.74	57.18	154.61	0.11	C25n 0.216	56.78	56.01	56.78	57.22
Tc	Sphenolithus anarrhopus				8.62	0.49	C25n 0.331	56.84	56.07	56.84	57.28	155.03	0.11	C25n 0.283	56.81	56.04	56.81	57.26
B	Discoaster delicatus gr.				6.86	0.12	C25n 0.583	56.97	56.19	56.97	57.42	156.92	0.11	C25n 0.583	56.97	56.19	56.97	57.42
B	B1/B2 base				5.41	0.10	C25n 0.791	57.08	56.29	57.07	57.54	158.37	0.02	C25n 0.813	57.10	56.30	57.08	57.08
B	Ericsonia robusta				3.97	0.07	C25n 0.998	57.20	56.39	57.18	57.65	158.00	0.11	C25n 0.754	57.06	56.27	57.05	57.55
	C25n base				3.96		0.000	57.197	56.391	57.180	57.656	159.55		0.000	57.197	56.391	57.180	57.64
B	Discoaster nobilis gr.		CP7		2.14	0.05	C25r	57.337	56.518	57.314	57.801	157.35	0.10	C25n 0.651	57.01	56.22	57.00	57.11
B	D. mohleri	NP7	CP6		–			–	–	–	–	171.50	0.11	C25r 0.984	58.53	58.53	58.53	58.53
B	C25r base				–		0.000	58.550	57.554	58.379	58.959	171.70		0.000	58.550	57.554	58.379	58.959

Reference calcareous nannofossil biozonations: [a] NP (Martini, 1971); [b] CP (Okada and Bukry, 1980); [c] CN (Agnini et al., 2014). Reference timescales: W01 (Westerhold et al., 2008 – option 1); CK95 (Cande and Kent, 1995); GTS04 (Ogg and Smith, 2004); GTS12 (Ogg, 2012); DAMR09I (Dallanave et al., 2009); AG07+ (Agnini et al., 2007b).
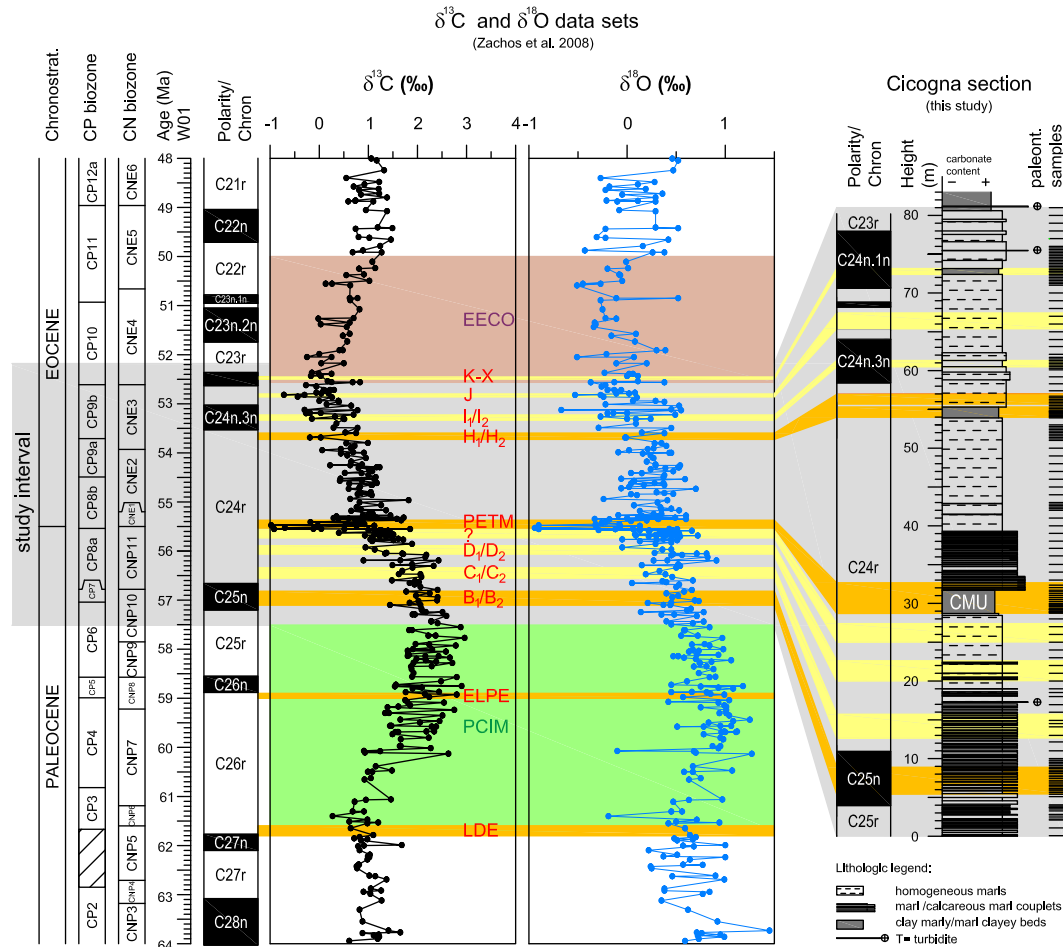
Figure 1. Middle Paleocene to middle Eocene (64 to 48 Ma) stable isotope ($\delta^{13}C$ and $\delta^{18}O$) records of benthic foraminifera from multiple locations (Zachos et al., 2008) placed on the option 1 (W01) timescale of Westerhold et al. (2008). Also shown are positions of polarity chrons and calcareous nannofossil biozones for this time interval, both from the CP biozone scheme (Okada and Bukry, 1980) and the CN biozone scheme (Agnini et al., 2014). Various "events" are noted within this chronostratigraphic framework, including the Paleocene carbon isotope maximum (PCIM), the Paleocene–Eocene Thermal Maximum (PETM), the H-1/ETM-2 event, the K/X event, and the Early Eocene Climatic Optimum (EECO). To the right is the general lithologic column and magnetostratigraphy of the Cicogna section (Dallanave et al., 2009).

While numerous studies have examined calcareous nanno-fossils across the PETM from different perspectives (e.g., Bralower, 2002; Stoll and Bains, 2003; Gibbs et al., 2006a, b; Agnini et al., 2007a; Mutterlose et al., 2007; Bown and Pearson, 2009; Jiang and Wise, 2009; Self-Trail et al., 2012), the relationship between these organisms and carbon cycle perturbations before and after this short-lived warming episode remain poorly documented (Gibbs et al., 2012). It seems possible that the high rate of calcareous nannofossil taxonomic evolution (appearances and extinctions), as well as distinct changes in calcareous nannofossil abundance patterns, may provide excellent stratigraphic control across the early Paleogene (Bukry, 1973; Perch-Nielsen, 1985; Backman, 1986; Agnini et al., 2014). Moreover, if the exact relationship between changes in nannofossil assemblages and global carbon

cycle perturbations were known, key time intervals could be rapidly identified for more detailed work. Finally, changes in calcareous nannofossils across the early Paleogene provide insights about the response of an important part of the sediment forming marine biota to changes in climate and carbon cycling.

Very few stratigraphic sections presently have detailed and coupled records of stable isotopes, carbonate content, and calcareous nannofossil abundances across the broad late Paleocene–early Eocene interval. The two notable exceptions are Ocean Drilling Program (ODP) Site 1262 (southeast Atlantic; Agnini et al., 2007b; Zachos et al., 2010) and Deep Sea Drilling Project (DSDP) Site 577 (northwest Pacific; Shackleton, 1986; Dickens and Backman, 2013; Fig. 2). Here we present geochemical records ($\delta^{13}C$, $\delta^{18}O$ and $CaCO_3$

55 Ma reconstruction
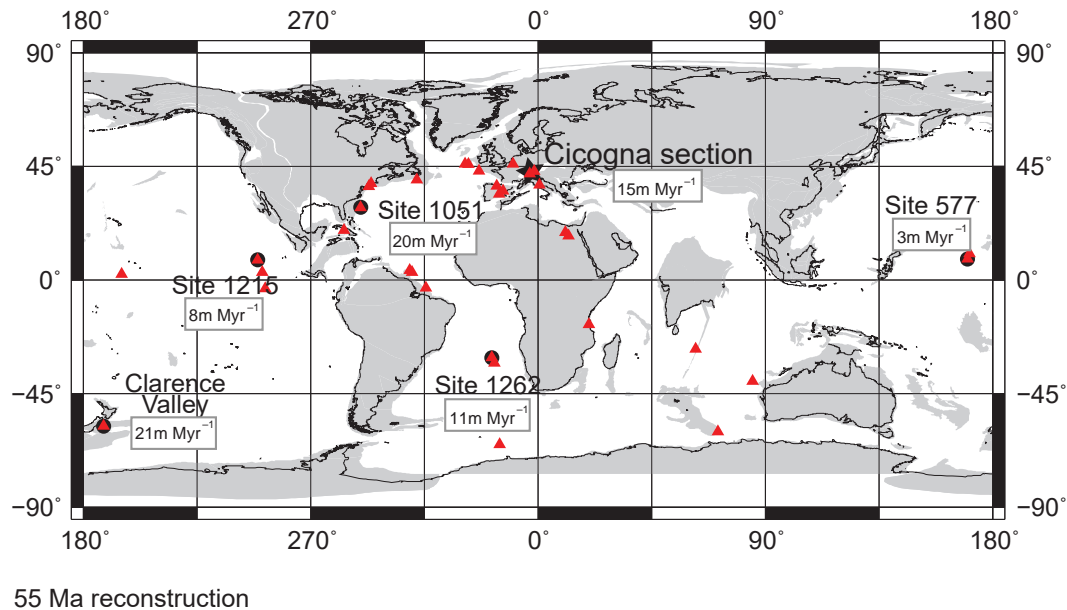
Figure 2. Paleogeographic map indicating approximate locations at 55 Ma for several key sites with detailed stable isotope records across the late Paleocene and early Eocene. These include (marked with black dots and star) the Cicogna section (NE Italy, this study), DSDP Site 577 (Shatsky Rise; Dickens and Backman, 2013), ODP sites 1051 (Blake Nose, Ogg and Bardot, 2001), 1215 (central Pacific; Raffi et al., 2005), and 1262 (Walvis Ridge; Westerhold et al., 2008), and the Clarence Valley (CV) sections (New Zealand; Slotnick et al., 2015b). The gray areas represent plate fragments, while the black lines show present-day shorelines. Boxes next to site locations show average sedimentation rates from the base of Chron C25n to the base of Chron C23r (57.20–52.36 Ma). The base map is from http://www.odsn.de/odsn/services/paleomap/paleomap.html. Red triangles are locations where a decrease in diversity of *Fasciculithus* spp. has been documented near the PETM. Locations include the Clarence Valley sections, central Pacific (ODP sites 1215, 1220, 1221), western Pacific (DSDP Site 577 and ODP Site 865), South Atlantic (Walvis Ridge, DSDP Site 527, ODP sites 1262, 1263–1267; Maud Rise, ODP Site 690), equatorial Atlantic (Ceara Rise, ODP Site 929, Demerara Rise, ODP sites 1259, 1260), northwestern Atlantic (New Jersey Margin land sections, ODP Site 1051, IODP Site U1403, U1409), northeastern Atlantic (Bay of Biscay DSDP sites 401, 549 and 550, Zumaya land section), and Indian Ocean (DSDP Site 213; ODP 672; Kerguelen Plateau, ODP Site 1135; Backman, 1986; Aubry, 1999a; Bralower, 2002; Dupuis et al., 2003; Tremolada and Bralower, 2004; Bralower and Mutterlose, 1995; Monechi et al., 2000; Gibbs et al., 2004; Raffi et al., 2005; Agnini et al., 2007a; Angori et al., 2007; Mutterlose et al., 2007; Jiang and Wise, 2009; Shamrock, 2010; Norris et al., 2014; Dallanave et al., 2015).

content) and calcareous nannofossil census data from the Cicogna section in northeast Italy (Figs. 2, 3). These data are compared with similar information from sites 1262 and 577. We show that the Cicogna section provides an important template for understanding potential relationships between climate, carbon cycling and the biotic evolution of calcareous nannoplankton.
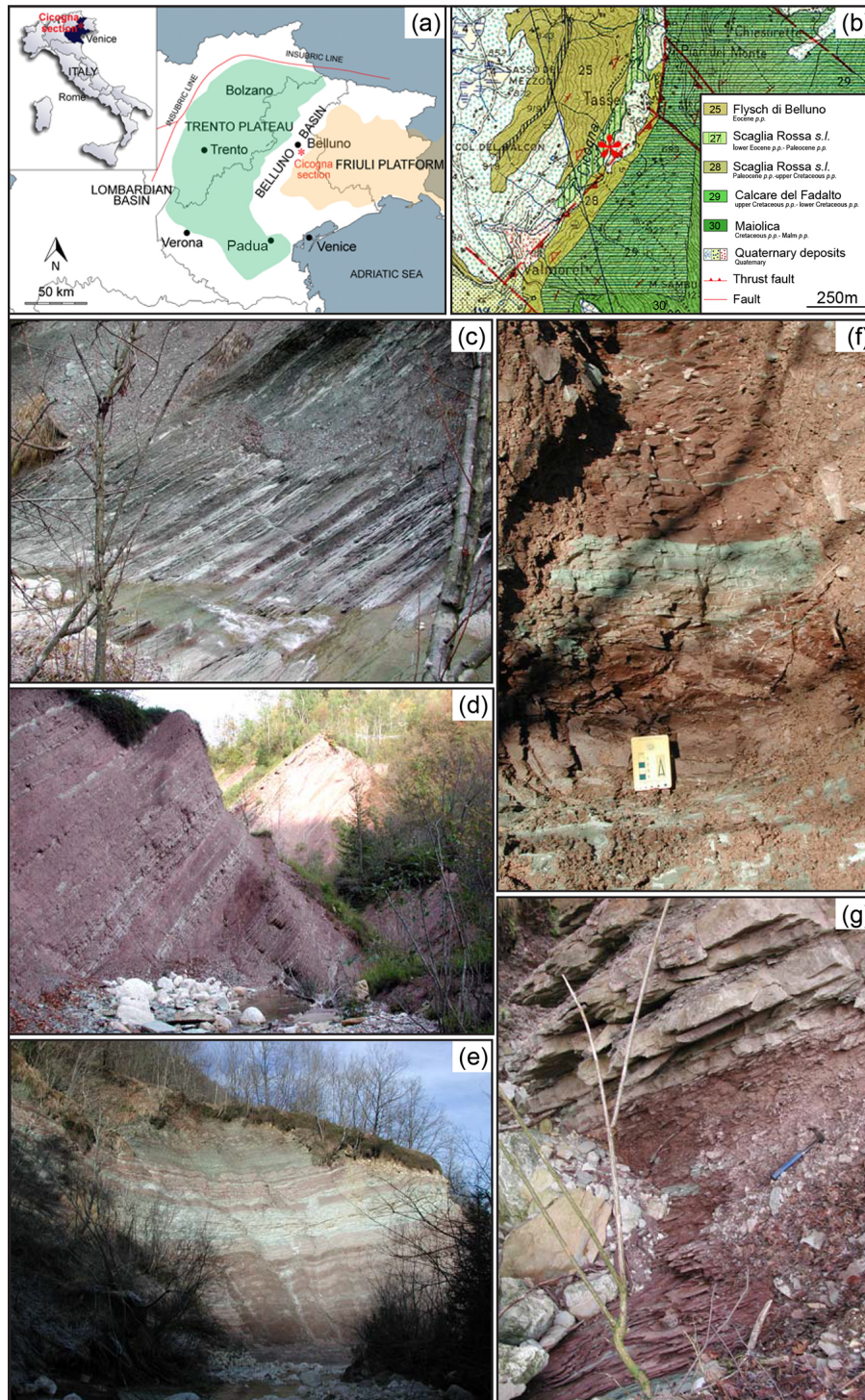
2 The Cicogna section

The Cicogna section crops out along the Cicogna Stream near the village of Tassei in Belluno Province, northeast Italy (Fig. 3). From a regional geological perspective, the sedimentary rocks of this section belong to the Belluno Basin. This basin represents part of a paleogeographic domain that formed when Jurassic rifting created a series of N–S-oriented structural highs (platforms) and lows (basins), which persisted through much of the Paleogene (Bernoulli and Jenkyns, 1974; Bernoulli et al., 1979; Winterer and Bosellini, 1981). Importantly, from the Cretaceous to the

middle–late Eocene, expanded deep sea sediment successions accumulated within the basins at nominally 30° N latitude (Stefani and Grandesso, 1991; Agnini et al., 2006, 2011; Zattin et al., 2006).

The Cicogna section consists of two lithostratigraphic units (Fig. 3). The lower portion is a well-exposed upper Paleocene and lower Eocene unit referred to as Scaglia Rossa sensu lato (Figs. 3, 4; Giusberti et al., 2007; Dallanave et al., 2009). Based on benthic foraminiferal assemblages, the early Paleogene marls of this unit represent lithified pelagic and hemipelagic sediment that accumulated at middle to lower bathyal water depth, likely between 600 and 1000 m and not deeper than 1500 m (Giusberti et al., 2007, 2016). The upper portion is a thick early to middle Eocene unit called the Belluno Flysch (Figs. 3, 4). This unit represents a synorogenic deposit on the flanks of the former Trento and Friuli platforms (Grandesso, 1976; Doglioni and Bosellini, 1987).

Once corrected for bed strike and dip (ca. 315° N; ca. 45°) and bends in the stream, the Scaglia Rossa at Cicogna measures 80 m in terms of stratigraphic height (Dallanave et al.,

Figure 3. The location and representative photographs of the Cicogna section in northeast Italy. **(a)** Geographic map showing the main Late Cretaceous–early Paleogene paleogeographic domains of the Italian Southern Alps (modified after Cati et al., 1989); **(b)** geological map of the local area (modified after Costa et al., 1996, indicating also the location of the Cicogna section; red asterisk); **(c)** alternating beds of Paleocene gray-green marls and calcareous marls (0–20 m); **(d)** the Scaglia Rossa sensu lato overlain by the Belluno Flysch; **(e)** marl/calcareous marl couplets in the lower Eocene portion of the section (approximately 40.0–70.0 m); **(f)** the base of the Clay Marl Unit, which denotes the onset of the PETM (approximately 28.7–29.3 m); and **(g)** the brownish-red interval of clayey marls with sporadic gray-green centimeter-scale spots and lenses, the CMU, overlain by prominent rhythmic alternations of marls and calcareous marls (approximately 28.7–33.0 m).
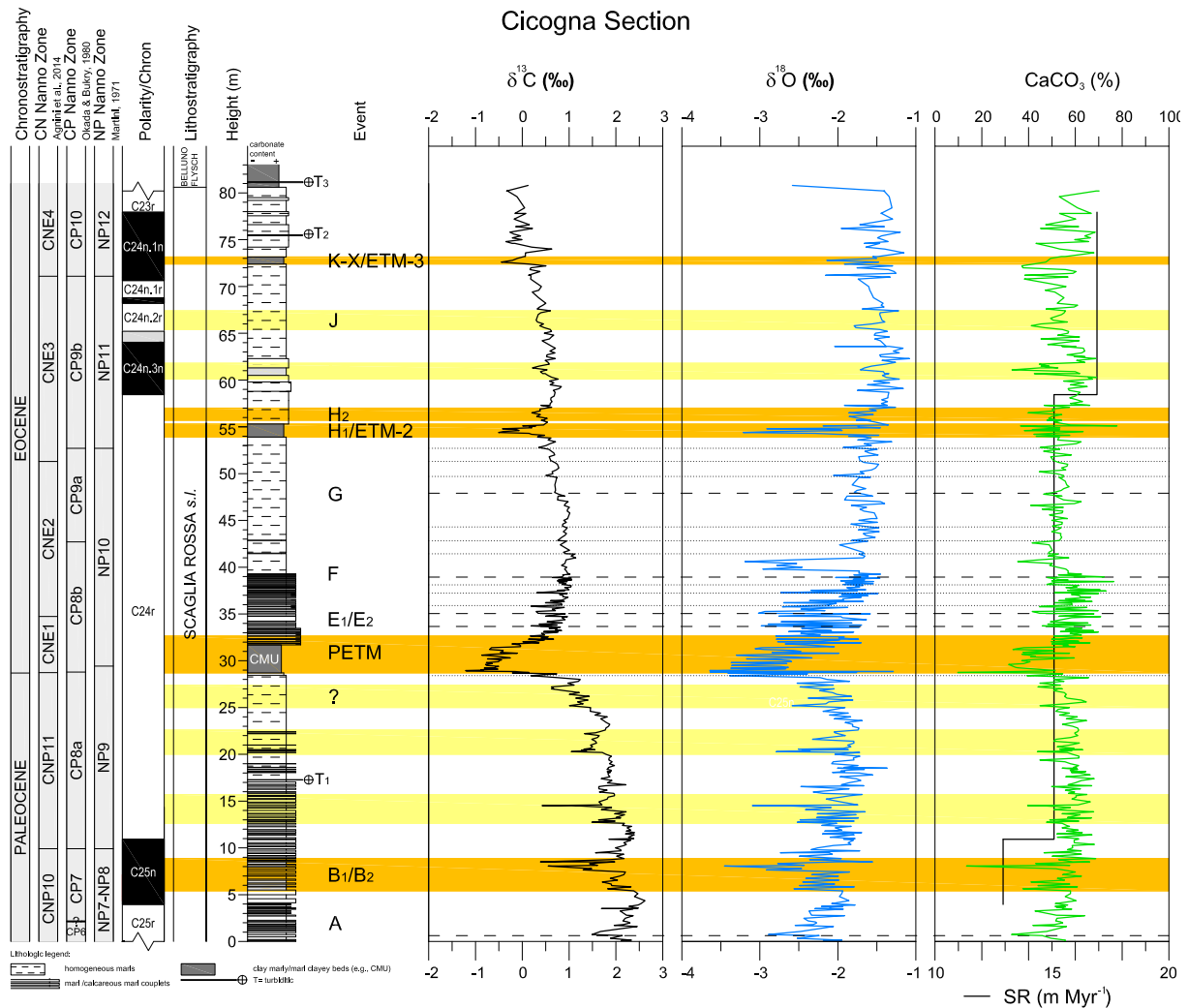
Figure 4. The Cicogna section with records of bulk carbonate δ^{13}C and δ^{18}O data, and CaCO$_3$ content. Calcareous nannofossil biostratigraphy (CP and NP biozones) and magnetostratigraphy are after Dallanave et al. (2009); CN biozones are also reported. Orange and yellow bands mark major δ^{13}C excursions. Dashed lines indicate minor CIEs that have been labeled elsewhere (e.g., E1/E2, F and G; Cramer et al., 2003), whereas dotted lines indicate minor changes in δ^{13}C that appear to occur also at ODP Site 1262 (see also Fig. 5).

2009). The Belluno Flysch measures 1 m in the Cicogna section. Furthermore, the section of interest can be subdivided into several subunits (Fig. 3). The lower 20 m is comprised of distinctive alternating beds of gray-greenish to purple marls and calcareous marls, the latter defined by carbonate contents higher than 60 % (Fig. 3c). This is overlain by approximately 9 m of pink-red marls with much less lithologic alternation. At 28.7 m, the sedimentary package is broken sharply by an approximately 3 m thick red to brownish-red interval of clayey marls with sporadic gray-green centimeter-scale spots and lenses (Fig. 3f, g). This has been called the Clay Marl Unit (CMU), and records the core of the prominent negative δ^{13}C excursion associated with the PETM at multiple outcrop sites within the Belluno Basin (Agnini et al., 2006, 2007a; Giusberti et al., 2007). Above the CMU, from 31.7 to

39.2 m, the section continues with deposition of rhythmic alternations of marls and calcareous marls (Fig. 3g). Above this 8.5 m thick interval, at ca. 40.5 m, spatic calcite crystals occur. Generally, couplets of marl and calcareous marl couplets become less evident from 40.5 until 54 m, where such couplets reoccur (Fig. 3d). At 75.5 m, a thin calcarenitic bed is encountered, presaging the onset of the Belluno Flysch. This turbidite is followed by a temporary return to hemipelagic sedimentation that ends at 80.6 m. Above, sedimentation of the Belluno Flysch begins in earnest (Figs. 3b, 4).

The basic stratigraphy of the Scaglia Rossa in the Cicogna section, including both polarity chron boundaries and key calcareous nannofossil biohorizons, has been published (Giusberti et al., 2007; Dallanave et al., 2009). The combined biomagnetostratigraphy indicates that the 81 m of in-

terest spans polarity Chron C25r to Chron 23r, and calcareous nannofossil biozones CP6 to CP10 (Okada and Bukry, 1980) or CNP10 to CNE4 (Agnini et al., 2014). Thus, the section represents a 5.3-million-year- (Myr) long time interval, from about 57.5 to 52.2 Ma on the W0-1 timescale. This also implies an average sedimentation rate (SR) of ca. 15 m Myr^{-1}. Although the deposition of hemipelagic sediment might suggest relatively constant SRs over time, the PETM and possibly other hyperthermal events in the Belluno Basin were characterized by higher SRs (Giusberti et al., 2007; Agnini et al., 2009; Tipple et al., 2011; Krishnan et al., 2015).

The Scaglia Rossa at Cicogna appears to record fairly continuous sediment accumulation at moderately high deposition rates. This is important because it affords longer time duration than most shallow ocean sites, greater time resolution than most deep ocean sites (Fig. 2), and an overall different environmental setting. Many early Paleogene records, especially those from paleo-shelf environments, such as in Egypt (e.g, Aubry and Salem, 2012) and New Jersey (Mixon and Powars, 1994; Harris et al., 2010), or from early deep sea drilling expeditions, such as in the Indian Ocean (Slotnick et al., 2015b), are discontinuous, because of either hiatuses or core gaps. Much of the detailed work and current understanding of stable carbon isotope stratigraphy and calcareous nannofossil variations across the broad early Paleogene, therefore, has come from deep-sea drilling sites with multiple holes but slow sedimentation rates, although we note the work in Clarence Valley, New Zealand (Fig. 2), another area that contains several paleo-slope sections with moderately high sedimentation rates (Nicolo et al., 2007; Slotnick et al., 2012, 2015b; Dallanave et al., 2015). For the Cicogna section, detailed stable isotope and CaCO$_3$ records are currently lacking, as well as detailed calcareous nannofossil assemblage information, which we present here.

3 Material and methods

3.1 Samples

A total of 492 samples were chiseled from outcrops along the section. Samples were selected so as to be as fresh and unaltered as possible. This included chipping off weathered surfaces while in the field. Each sample was calibrated to height (Fig. 4). Samples then were split, with one portion powdered in an agate ball mill, and subsequently freeze-dried.

3.2 Geochemistry

Each of the powdered samples was analyzed for bulk sediment stable isotope composition at the Stable Isotope Laboratory, University of Southampton, UK. A known mass ($\sim 80\,\mu g$) was placed into a headspace vial, dried overnight, and flushed with helium. To each sample, 10 mL of 100 % phosphoric acid was added and allowed to react. The lib-

erated CO$_2$ gas was measured using an EUROPA Scientific GEO 20–20 mass spectrometer fitted with a microCAPS for carbonate analysis. Results are reported in standard delta notation relative to Vienna Pee Dee Belemnite (VPDB). An in-house standard of Carrara marble, calibrated to NBS-19 limestone, was measured multiple times to evaluate accuracy and precision. The external analytical precision (1σ), based on these replicate analyses, was 0.028 ‰ for δ^{13}C and 0.057 ‰ for δ^{18}O.

The amount of CaCO$_3$ in each sample was calculated from the beam height response during isotope mass spectrometer measurements (Spofforth et al., 2010). The liberated CO$_2$ gas, when squeezed up in the bellows, is measured and generates a current, the beam height. The pressure of CO$_2$ gas is directly proportional to the beam height and therefore the mass of carbonate in the sample. Over 100 samples of pure CaCO$_3$, with masses between 200 and 480 μg, were analyzed to establish a linear relationship between beam height and carbonate content (CaCO$_3$ = $mx + b$; $R^2 = 0.94$–0.99). Results were validated by analyzing 30 samples on a C-H-N-O elemental analyzer.

3.3 Calcareous nannofossils

The un-powdered sample split was examined for calcareous nannofossils. Raw sediments were processed to prepare standard smear slides (Bown and Young, 1998). To assess the reproducibility of our counting methods in every single sample, a pivotal sample was prepared 10 times by two different operators. Repeated counts of the identical sample performed by different analysts gave similar results (sd < 2–5 %). Particle density estimates (Baccelle and Bosellini, 1965) were not carried out because samples have a high range in the terrigenous content (22 to 90 %). An increase or decrease in the silicoclastic component is mainly related to the major or minor efficiency of the chemical and mechanical weathering on land (Agnini et al., 2009). In the studied sediments, the variation in the amount of the terrigenous content through time has modified the density of the allochemic particle component. Consequently, calcareous nannofossil absolute abundances could not be estimated correctly using a homogeneous/constant particle density or by weighing the same amount of sediment for each smear slide. However, the scope of semi-quantitative counts performed in this study is to recognize the precise position of biostratigraphic biohorizons rather than use these data as a proxy of the paleoproductivity of taxa. Essentially, the identification of the appearance or disappearance of any given taxon is not affected by its stratigraphic abundance pattern, which obviously reduces the negative effect of the variable abundance of the silicoclastic component throughout the section. Samples were examined under a Zeiss light microscope at 1250× magnification. Calcareous nannofossils were determined using taxonomy proposed by Aubry (1984, 1988, 1989, 1990, 1999b), Perch-Nielsen (1985) and Bown (2005).
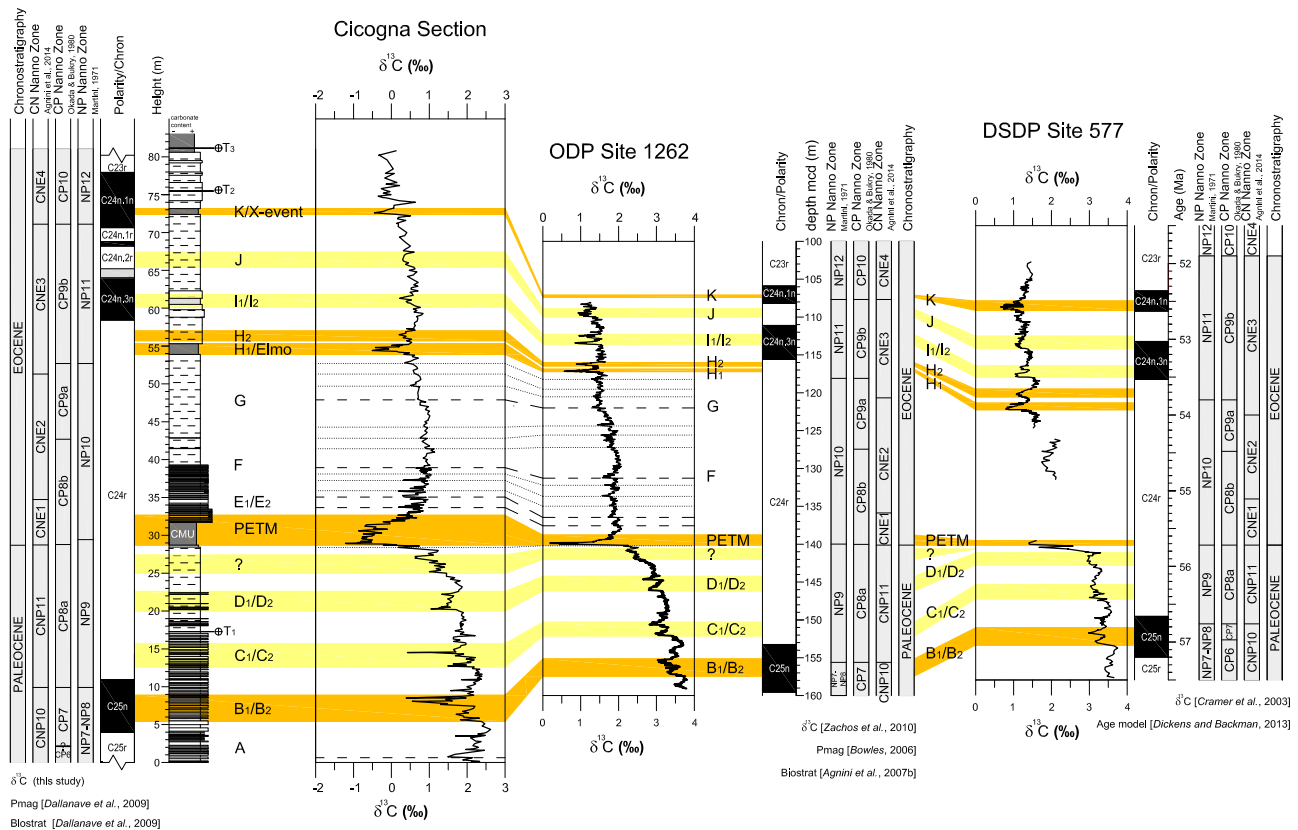
Figure 5. Stratigraphic correlation between upper Paleocene and lower Eocene sections at Cicogna, ODP Site 1262 (Zachos et al., 2010), and DSDP Site 577 (Cramer et al., 2003; Dickens and Backman, 2013). All three sites have independently derived nannofossil biohorizons, polarity chrons and $\delta^{13}C$ records, which account for subtle temporal offsets. Color bands and symbols are the same as in Fig. 4. Note the missing record at Site 577 that corresponds to known core gaps.

A total of 200 samples were examined, providing an average time resolution of ca. 25 kyr. A preliminary qualitative estimate of the abundance and preservation state of calcareous nannofossil assemblages was performed for all samples. An initial large batch (185) was analyzed primarily to provide biostratigraphic control for the Cicogna section, and the basic results have been presented by Dallanave et al. (2009). We re-checked and refined the positions of some biohorizons by examining 15 additional samples, primarily across some of the CIEs, such as B1/B2, PETM, H1 and H2, and K/X (Cramer et al., 2003). The calcareous nannofossil biostratigraphic schemes used by Dallanave et al. (2009) were those of Martini (1971) and Okada and Bukry (1980). The new zonal scheme of Agnini et al. (2014) is also used here. Biohorizon nomenclature follows that given by Agnini et al. (2014): base (B), base common (Bc), top (T) and top common (Tc).

Calcareous nannofossil biostratigraphic results are based on semi-quantitative analyses, which is based on counts of the number of specimens of selected taxa present in a prefixed area, $1\,mm^2$ or three long traverses (modified after Backman and Shackleton, 1983). Calcareous nannofossil paleoecological results are instead based on relative abundances of calcareous nannofossil taxa (percent of the total assemblage), calculated from counts of at least 300 specimens.

To capture changes in calcareous nannofossil assemblages we also use a statistical approach. Principal component analysis (PCA) was preferred to other methods, such as the non-metric multidimensional scaling (MDS) procedure, for which a small number of axes are chosen prior to the analysis and the data are fitted to these dimensions (Hammer et al., 2001). However, non-metric MDS results were performed and are available as Supplement (Fig. S2). Multivariate analysis of variance (MANOVA) was carried out on our data set to determine whether significative differences are present among the three groups of samples recognized with PCA.

PCA and MANOVA were performed on the percentages of 15 subgroups using the statistical software package PAST ver. 2.17c (Hammer et al., 2001). The former analysis is often used for examining paleontological data (e.g., Buccianti et al., 2006; Kucera and Malmgren, 1998; Watkins and Self-Trail, 1992; Thibault and Gardin, 2010; Marino et al.,

2008; Bordiga et al., 2015), as it can point out hypothetical variables (components) that explain much of the variance in a multidimensional data set. The first principal component accounts for the most variability in any data set examined. Each succeeding component has the highest variance possible relative to the preceding components (Hammer et al., 2001). This method also increases the symmetry, homoscedasticity and linearity of the data set (Aitchison, 1986). The chosen subgroups were *Chiasmolithus*, *Coccolithus*, *Ellipsolithus*, *Discoaster*, *Ericsonia*, *Fasciculithus*, *Girgisia*, *Octolithus*, *Prinsius*, *Sphenolithus*, *Toweius*, *Rhomboaster/Tribrachiatus*, *Zyghrablithus*, reworked forms, and "others".

4 Results

4.1 Carbon isotopes

The bulk rock δ^{13}C record for the Cicogna section can be described, in a general sense, as a long-term decrease of approximately 3 ‰, punctuated by a series of negative CIEs (Fig. 4). The most prominent low in δ^{13}C coincides with the CMU.

Previously established polarity chron boundaries and key calcareous nannofossil biohorizons at the Cicogna section (Dallanave et al., 2009) provide a very good stratigraphic framework. Once placed onto a common timescale, in this case WO-1 (Westerhold et al., 2008), the δ^{13}C record at Cicogna is fairly similar to those records generated using upper Paleocene and lower Eocene marine carbonate at other locations (Cramer et al., 2003; Zachos et al., 2010; Slotnick et al., 2012). This includes, for example, bulk carbonate δ^{13}C records at ODP Site 1262, and DSDP Site 577 (Fig. 5) The relatively high δ^{13}C values near the base of the Cicogna section document the late stages of the PCIM, which was centered within C25r (Fig. 1). The overall drop in δ^{13}C across the section marks the long-term global decrease in δ^{13}C that lasted through Chron C24n (Fig. 1). The record contains multiple negative shifts in δ^{13}C. There is, however, an intriguing difference: across the Cicogna section, the long-term 3 ‰ shift in bulk carbonate δ^{13}C values is generally offset from that in bulk carbonate δ^{13}C records at sites 1262 and 577 by approximately -1 ‰.

The superimposed CIEs are considered to correspond to CIEs found in δ^{13}C records from elsewhere, some of which represent known or inferred hyperthermal events (Cramer et al., 2003; Lourens et al., 2005; Nicolo et al., 2007; Zachos et al., 2010; Slotnick et al., 2012). There are three pairs of CIEs below the CMU (Fig. 4), as well as during the initial upper Paleocene long-term decline in δ^{13}C. These correspond to the B1/B2, C1/C2 and D1/D2 CIEs documented by others (Cramer et al., 2003; Zachos et al., 2010). Notably, at Site 1262, the B1/B2 CIEs occur during middle C25n, and the C1/C2 CIEs occur at the start of C24r (Fig. 5). The same is true at Cicogna. Interestingly, at Cicogna, the B2 and C2
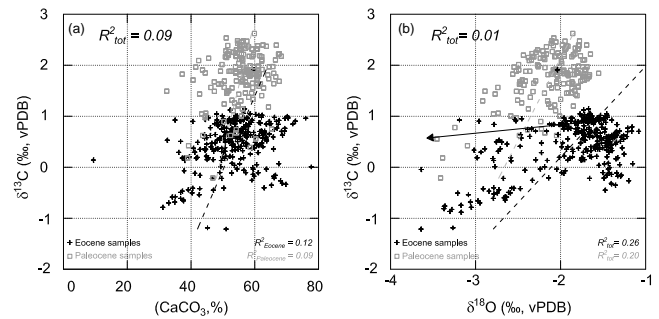
Figure 6. Plots of **(a)** bulk carbonate δ^{13}C versus bulk oxygen δ^{18}O and **(b)** bulk carbonate δ^{13}C vs. CaCO$_3$ content for samples from the Cicogna section. The black arrow shows the expected effect of burial diagenesis. Grey and black dash lines are linear trend lines for Paleocene and Eocene samples, respectively. Note the clear distinction in δ^{13}C for Paleocene and Eocene samples, which relates to a long-term decrease in δ^{13}C (Fig. 5).

CIEs show greater magnitudes than the B1 and C1 CIEs, and these paired excursions are more pronounced than at all other locations examined to date. An additional paired CIE occurs in the uppermost Paleocene (Fig. 4). This may correlate to a fourth set of late Paleocene CIEs documented at Site 1262 (Zachos et al., 2010).

The lower Eocene portion of the δ^{13}C record at Cicogna (Fig. 4) begins at the CMU, which marks the PETM (Giusberti et al., 2007; Dallanave et al., 2009). As at many locations, the PETM is characterized by a prominent negative CIE. The shift in δ^{13}C at Cicogna is approximately -2.5 ‰, a decrease that begins abruptly at 28.7 m and returns more gradually to near pre-excursion values by about 33 m. From approximately 33 to 54 m, the δ^{13}C curve shows a relatively smooth trend. At 54 m, a pair of CIEs begin, with the first pair having a magnitude of about 1.0 ‰. These are the H1/H2 events (Cramer et al., 2003), which occurred in the upper part of Chron C24r (Lourens et al., 2005; Zachos et al., 2010; Dickens and Backman, 2013; Dallanave et al., 2015). Above the H1/H2 CIEs, and within Chron C24n, are a series of smaller (0.4 to 0.6 ‰) CIEs. Those at approximately 60, 65 and 72 m are correlated with the I1/I2, J and K/X events, respectively. In summary, the δ^{13}C record at Cicogna correlates with that at ODP Site 1262 (Zachos et al., 2010) and DSDP Site 577 (Dickens and Backman, 2013; Fig. 5), as well as at several other locations (Cramer et al., 2003; Slotnick et al., 2012, 2015b). This is important because it enables comparison and discussion between widely separated sedimentary records within a firm temporal framework.

4.2 Oxygen isotopes

The δ^{18}O values range from -1.08 to -3.64 ‰ with a mean value of -1.96 ‰ and a standard deviation (1σ) of 0.50 ‰ (Fig. 4). However, at the broad scale, δ^{18}O increases upsection, with Paleocene samples averaging -2.10 ‰ and Eocene

samples averaging $-1.89\,‰$. This trend is noteworthy because $\delta^{18}O$ values should decrease upsection if the composition of the $CaCO_3$ was principally reflecting rising global temperatures through the early Eocene. The 1σ of $\delta^{18}O$ values also increases upsection, being $0.33\,‰$ across Paleocene samples and $0.56\,‰$ across Eocene samples.

There is virtually no correlation ($r^2 = 0.014$; $r = 0.12$) between $\delta^{18}O$ and $\delta^{13}C$ values across all samples (Fig. 6). However, most "short-term" CIEs do display decreases in $\delta^{18}O$ (Fig. 4). An interval of anomalously low $\delta^{18}O$ values occurs from 39.9 to 40.9 m, where the spatic calcite was observed.

4.3 Carbonate content

The $CaCO_3$ content varies between 9.4 and 77.7 % across the sample suite, with a mean value of 54.3 % and a 1σ of 8.2 % (Fig. 4). Two important findings emerge from the $CaCO_3$ content record. First, from 39 to 54 m, where we find limited variance in the $\delta^{13}C$ curve, $CaCO_3$ content averages 52.1 % with a 1σ of 4.9 %. Thus, while the average is similar to that calculated for the entire section, the standard deviation is much less. At Site 1262, the corresponding time interval is also characterized by limited variance in $\delta^{13}C$ values and carbonate contents, the latter inferred from the abundance of Fe counts in XRF scans (Zachos et al., 2010). Second, across all samples, the $CaCO_3$ content covaries somewhat ($r = 0.29$) with $\delta^{13}C$ (Fig. 6). This is because several lows in $CaCO_3$ content coincide with minima in $\delta^{13}C$, as is obvious for the B1/B2, PETM and H1/H2 events (Fig. 4).
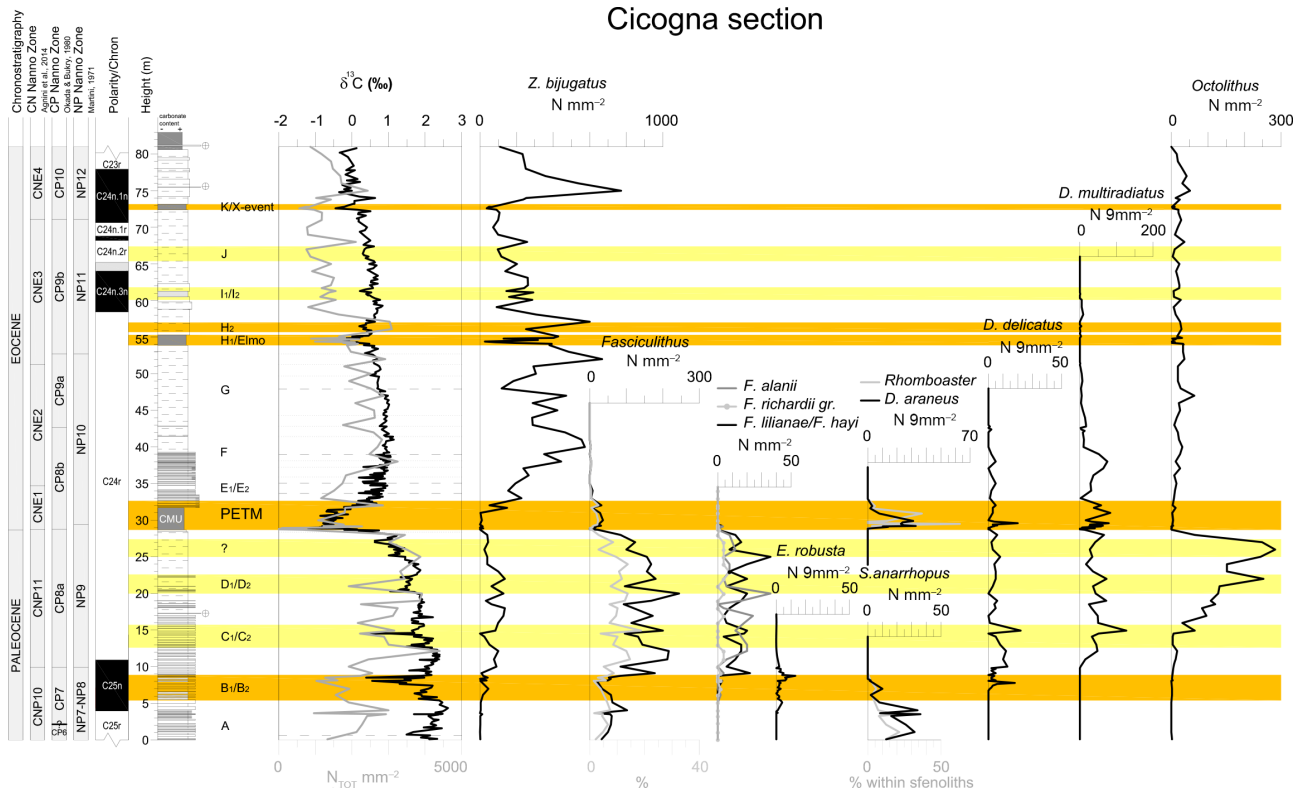
4.4 Calcareous nannofossils

Calcareous nannofossils are generally abundant, diverse, and moderately well preserved. The sole exception is across a 10 cm interval from 28.75 to 28.85 m, which corresponds to the onset of the CIE that marks the PETM. The three samples from this interval are virtually barren of calcareous nannofossils.

Secondary overgrowth of calcite can partially or wholly blur species-specific morphological features. Such diagenetic alteration, however, only marginally influences the relative, semi-quantitative and absolute abundance of calcareous nannofossil taxa (Toffanin et al., 2013). Calcite dissolution, on the other hand, can significantly affect the relative abundances of various calcareous nannofossils within a given volume of sediment. This is because the removal of more dissolution susceptible taxa, such as *Toweius* and holococcoliths, necessarily increases the abundance of less dissolution susceptible taxa, such as discoasters (Roth and Thierstein, 1972; Adelseck et al., 1973; Roth, 1983; Bornemann and Mutterlose, 2008; Toffanin et al., 2013). In general, moderate to strong calcite dissolution also decreases the total abundance of calcareous nannofossils within a given volume of sediment (Adelseck et al., 1973; Toffanin et al., 2011). In the Cicogna section, calcite overgrowth on discoasters
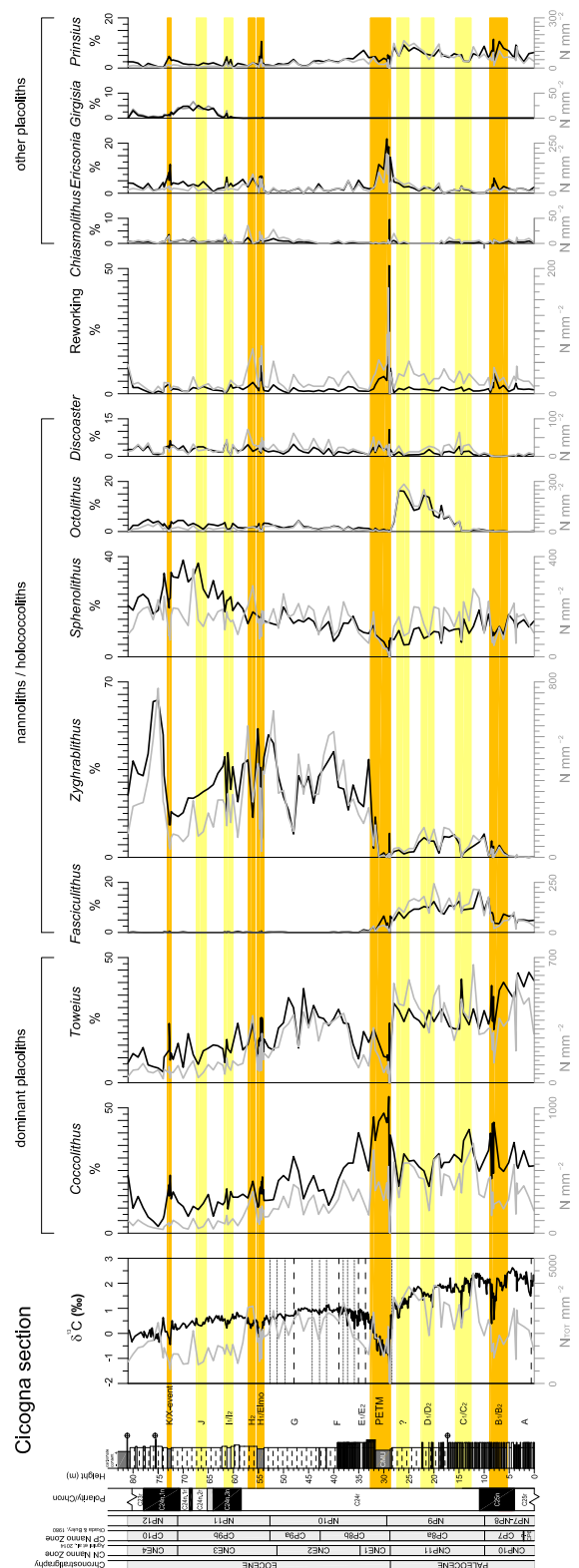
Figure 7. Relative (%) and semi-quantitative (N mm^{-2}) abundances of selected calcareous nannofossil genera across the Cicogna section. Also shown are the lithostratigraphy, magnetostratigraphy, biostratigraphy and carbon isotope ($\delta^{13}C$) stratigraphy at the Cicogna section (Fig. 4). Color bands and symbols are the same as in previous figures.

Figure 8. Relative (%) and semi-quantitative (N mm^{-2}) abundances of selected, mainly late Paleocene, calcareous nannofossil taxa across the Cicogna section. Also shown are the lithostratigraphy, magnetostratigraphy, biostratigraphy and carbon isotope (δ^{13}C) stratigraphy at the Cicogna section (Fig. 4). Color bands and symbols are the same as in previous figures.
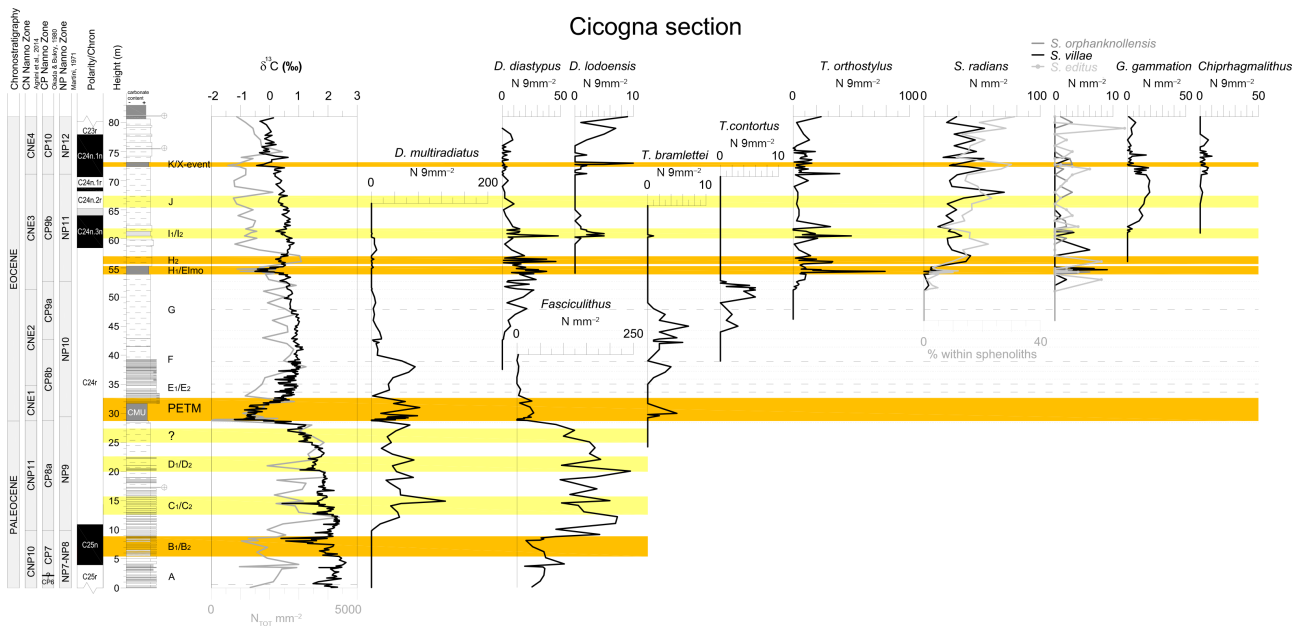
Figure 9. Relative (%) and semi-quantitative (N mm^{-2}) abundances of selected, mainly early Eocene, calcareous nannofossil taxa across the Cicogna section. Also shown are the lithostratigraphy, magnetostratigraphy, biostratigraphy and carbon isotope (δ^{13}C) stratigraphy at the Cicogna section (Fig. 4). Color bands and symbols are the same as in previous figures.

is the prevalent process affecting calcareous nannofossil assemblages (Plate I). Most assemblages display high abundances (> 1000 specimens mm^{-2}) and a high diversity, which include more fragile taxa. It follows that dissolution has not severely altered most assemblages in samples from the Cicogna section. Rather, the calcareous nannofossil record is considered to represent a genuine paleoecological signal.

Nannofossil assemblages from the Cicogna section display several general trends (Figs. 7–9). At the most basic level, there is a decrease in the total number of nannofossils ($N mm^{-2}$) with decreasing age. Paleocene samples average approximately 2600 specimens mm^{-2}, whereas Eocene samples above the H1/H2 events average approximately 1200 specimens mm^{-2}. This decrease in abundance broadly corresponds to a change in calcareous nannofossil composition, as supported through a series of additional observations at the Cicogna section (Figs. 7–9):

– *Coccolithus* and *Toweius* constitute nearly half of the assemblages considering the entire section. However, these genera show a clear decrease in abundance upsection, with a mean value of 60 % in Paleocene samples and 35 % in Eocene samples.

– *Zyghrablithus bijugatus* shows a low mean value of approximately 4 % in the Paleocene, followed by a sharp increase in the basal part of the Eocene, and a mean value of approximately 25 % upsection in the Eocene. Hence, the abundance of this taxon expands on behalf of *Coccolithus* and *Toweius*.

– *Sphenolithus* decreases progressively during the Paleocene, suddenly disappears at the onset of the PETM, before returning to and exceeding pre-PETM values in the lower Eocene. Thus, the abundance of sphenoliths also expands on behalf of *Coccolithus* and *Toweius*.

– *Fasciculithus* shows a severe decline in abundance and species diversity at the onset of the PETM (28.70 m), leading up to their extinction at 34.73 m.

– *Octolithus* is rare throughout most of the studied section, but displays high abundances from approximately 14.7 to 27.5 m in the upper Paleocene.

– *Discoaster* does not show any distinct change in abundance except for a single peak at the onset of the PETM.

– Several Cretaceous and early Paleocene species constitute minor reworked components throughout the section. Notably, the intervals marked by the PETM, H1/H2 and, to a lesser extent, B1/B2 CIEs are characterized by higher abundances of these reworked components.

– Representatives of placolith genera, such as *Prinsius*, *Ericsonia*, *Chiasmolithus* and *Girgisia*, are minor components of most samples. *Prinsius* displays a marked permanent decrease in abundance from a mean value of approximately 6 to 2.5 % across the Paleocene–Eocene boundary. By contrast, *Ericsonia* does not show a prominent difference in abundance between Paleocene and Eocene assemblages, but increases in abundance during known and suspected hyperthermal events.

– The calcareous nannofossil excursion taxa (CNET), which include *Discoaster araneus* and the genus *Rhomboaster* are present during the CIE of the PETM. The evolution of the *Rhomboaster/Tribrachiatus* plexus started at the onset of the PETM, when *Rhomboaster* and *T. bramlettei* first appeared, and continued into the lower Eocene with the successive appearances of *T. contortus* and *T. orthostylus* (Raffi et al., 2005; Agnini et al., 2006, 2007b).

Beyond the above variations, evolutionary appearances and extinctions occur during the studied time interval (Figs. 7–9). Most of these species belong to *Discoaster*, *Sphenolithus* and the *Rhomboaster/Tribrachiatus* lineage, and include *D. multiradiatus*, *D. diastypus*, *D. lodoensis*, *S. radians*, *S. anarrhopus*, *T. bramlettei*, *T. contortus* and *T. orthostylus*. The biohorizons defined using these species are exceptionally useful for biostratigraphy and, interestingly, often occur close to changes in $\delta^{13}C$.

All assemblage data were used for PCA. This indicates that PC1 (41.3 %) and PC2 (14.7 %) together account for 56 % of the variance in the data set. The PCA graph (Figs. 10a, S1) shows that samples can be subdivided into three subgroups. The first two populations of samples are distinguished because of their different positions along the x axis (PC1). The third population is much more dispersed but a possible discrimination from the other two seems to be hypothesized because of its different position along the y axis (PC2). The use of a different statistical procedure, such as non-metric MDS, does not substantially change these results (Fig. S2). To further support the subdivision of the study samples in three subgroup, we applied MANOVA to our data set (Fig. 10b). The result clearly confirmed that Paleocene, PETM and Eocene samples are in fact isolated one from each other.

5 Discussion

5.1 Integrated stratigraphy and a carbon isotope template

Polarity chron boundaries and calcareous nannofossil biohorizons (Table 1; Fig. 4) provide a solid stratigraphic framework for the Cicogna section. Calcareous nannofossil biohorizons, including additional ones defined here, align in same stratigraphic order when compared to other locations, such as ODP Site 1262 and DSDP Site 577 (Table 1; Fig. 11). The Cicogna section represents sediment accumulation between 57.5 and 52.2 Ma on the WO-1 timescale (Dallanave
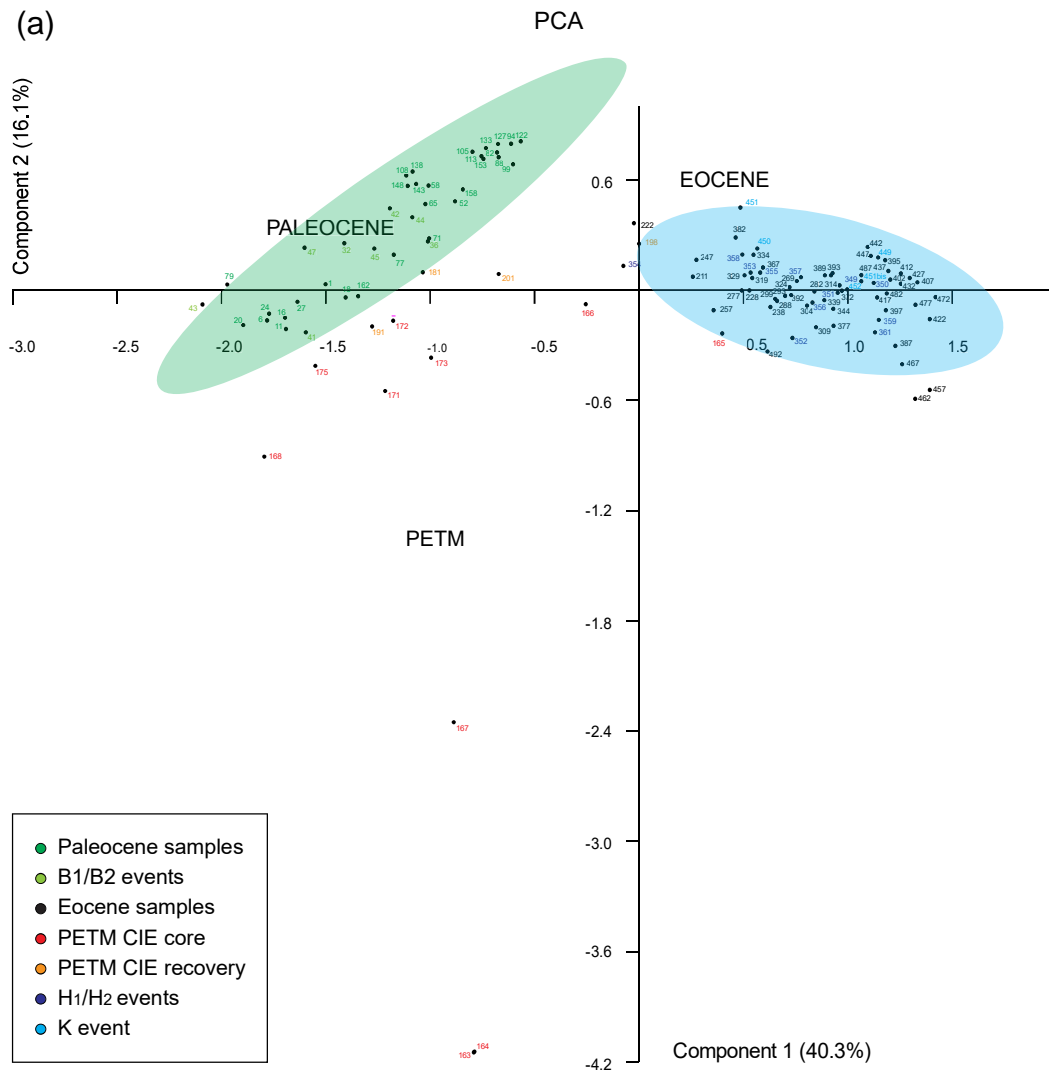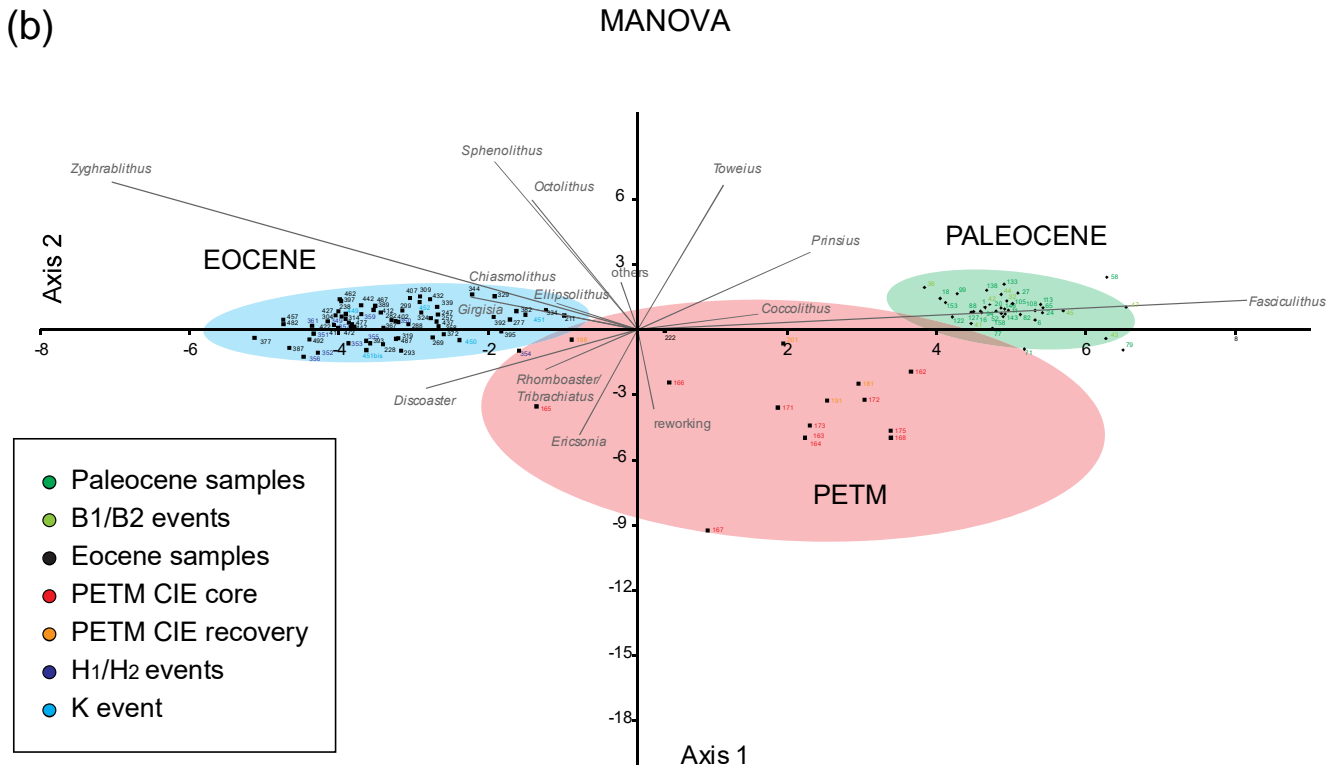
Figure 10.

et al., 2009). The average SR was ca.15.2 m Myr^{-1}, although this must have varied (Figs. 3, 11). The CMU, which marks the "core" of the PETM and ca. 80–100 kyr, showing a higher sedimentation rate than much of the remaining record (Dallanave et al., 2009; Krishnan et al., 2015).

Once placed into the above stratigraphic framework, the bulk carbonate δ^{13}C profile documented at Cicogna correlates well with that generated at ODP Site 1262 (Fig. 5). In fact, it is similar to δ^{13}C profiles generated at multiple locations (Figs. 2, S4), as long as records have been properly calibrated in both the depth and time domains. This includes accounting for core stretching and core gaps at scientific drilling sites, such as at DSDP Site 577 (Dickens and Backman, 2013), and accounting for changing strike and dip along land sections, such as done at Cicogna (Fig. 3). During late Paleocene and early Eocene times, the Cicogna section records the long-term decrease in δ^{13}C. Superimposed

on this drop were multiple, often paired, negative CIEs. The PETM definitively represents the most prominent CIE, but several other CIEs occurred before and after. Importantly, the relative positions of polarity chron boundaries, key calcareous nannofossil biohorizons and CIEs at Cicogna align well with those found at other locations (Table 1; Figs. 5, 11).

A clearly recognizable δ^{13}C pattern spans the late Paleocene through the early Eocene at several locations (Cramer et al., 2003; Nicolo et al., 2007; Galeotti et al., 2010; Zachos et al., 2010; Slotnick et al., 2012, 2015b), although the total number of CIEs remains uncertain. At Cicogna, the problem lies in the interval surrounding the K/X event, which broadly corresponds to the start of the EECO (see discussion in Slotnick et al., 2012). We cannot confirm with our sample resolution whether a series of short-term, small-amplitude CIEs mark this time, an idea suggested from δ^{13}C records of the Clarence Valley sections (Slotnick et al., 2012, 2015b). How-

Figure 10. Statistical Analyses of calcareous nannofossil percentage data of the Cicogna section. Calcareous nannofossils are subdivided into 15 subgroups (*Chiasmolithus*, *Coccolithus*, *Ellipsolithus*, *Discoaster*, *Ericsonia*, *Fasciculithus*, *Girgisia*, *Octolithus*, *Prinsius*, *Sphenolithus*, *Toweius*, *Rhomboaster/Tribrachiatus*, *Zyghrablithus*, reworking, others). **(a)** Principal component analysis (PCA) scatter plot of percentage data of calcareous nannofossil taxa of samples from the Cicogna section in terms of the first and second component. Each sample is represented by a circle and labeled. Green and blue shaded areas are the ellipses containing 95 % of the data points of Paleocene group and Eocene group, respectively. **(b)** Multivariate analysis of variance (MANOVA). Scatter graph and biplot. Each sample is represented by a black symbol (quadrangle and diamond) and labeled. Green, red and blue shaded areas are the ellipses containing 95 % of the data points of Paleocene group, PETM group and Eocene group, respectively.

ever, as at other locations, such as Site 1262, no significant CIEs occurred within the 1.6 Myr between the PETM and the H-1/ETM-2 event (Fig. 5).

The time-correlative δ^{13}C template implies changes in the mean ocean δ^{13}C of dissolved inorganic carbon (DIC). In turn, these compositional changes very likely represent variations in fluxes of highly ^{13}C-depleted carbon to and from the ocean or atmosphere, such as changes in the release and storage of organic carbon (Shackleton, 1986; Dickens et al., 1997; Kurtz et al., 2003; Deconto et al., 2010; Komar et al., 2013). The δ^{13}C record at Cicogna offers no direct insight on the location of this carbon (e.g., seafloor methane, permafrost, peat). However, it does support an important concept: the magnitudes of given CIEs appear somewhat related to one another and to the long-term δ^{13}C record. In particular, the PETM occurred about halfway between the long-term high and low in δ^{13}C, and heralded a relatively long time interval lacking CIEs. A generic explanation is that a very large mass of ^{13}C-depleted carbon was injected from some organic reservoir into the ocean or atmosphere during the PETM, and

that the reservoir needed to recharge for considerable time before the next injection (H-1/ETM-2) could occur (Dickens, 2003; Kurtz et al., 2003; Lunt et al., 2011; Komar et al., 2013).

The overall -1 ‰ offset of the δ^{13}C curve between the records at Cicogna and at sites 577 and 1262 (Fig. 5) warrants brief discussion. It probably does not reflect wholesale diagenesis and resetting of the primary signal at any of these sections. Otherwise, a recognizable correlative δ^{13}C record and well-preserved nannofossils (Plate I) would not be found at all three locations. In fact, it is difficult to modify the original δ^{13}C composition of carbonate over appreciable distance (greater than several meters) in marine sedimentary sequences dominated by fine-grained calcite, even those now exposed on land as lithified rock, such as at Cicogna or in the Clarence Valley. This is because the carbon water / rock ratio remains low, because almost all carbon exists in carbonate, and because temperature minimally influences carbon isotope fractionation (Matter et al., 1977; Scholle and Arthur, 1980; Frank et al., 1999). Instead, the offset in the
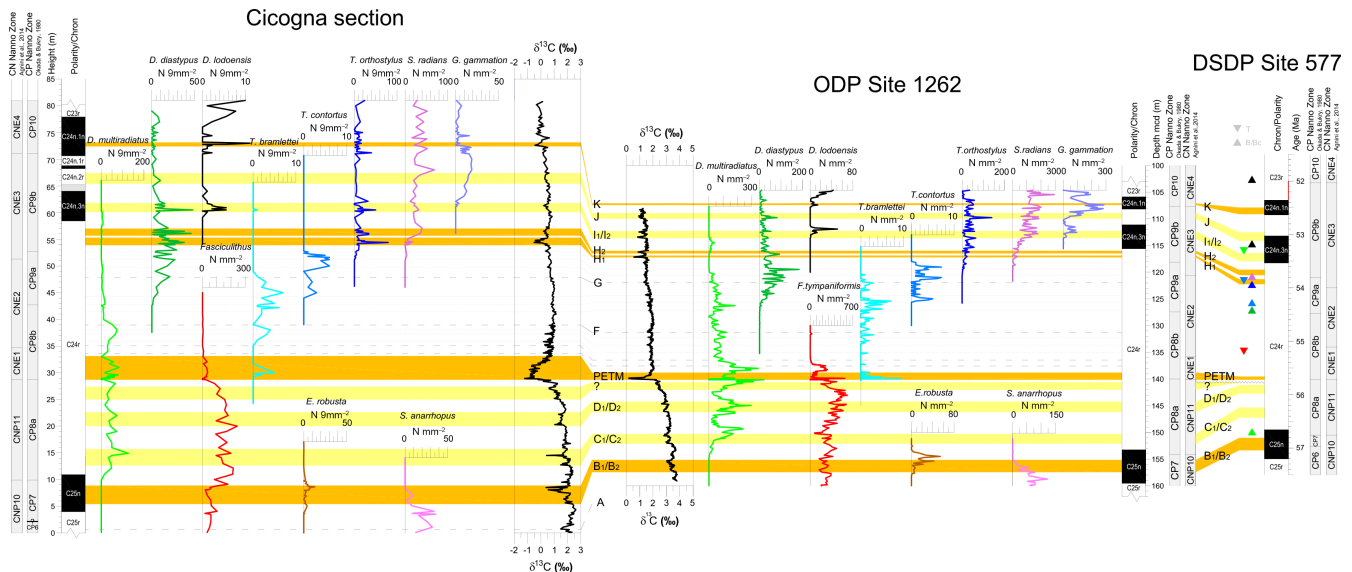
Figure 11. Comparison of δ^{13}C profiles and semi-quantitative abundance patterns of selected calcareous nannofossil taxa from the Cicogna section and ODP Site 1262. Calcareous nannofossil biohorizons from DSDP Site 577 are reported in the right part of the figure. Orange and yellow bands mark CIEs shown in previous figures. Color bands and symbols are the same as in previous figures.

δ^{13}C curves probably relates to differences in the composition of the original carbonate, a concept that we return to later.

However, local dissolution and re-precipitation of carbonate definitely has occurred in the Cicogna section. This can be observed in the overgrowths of secondary calcite on discoasters and *Rhomboaster/Tribrachiatus* (Plate I). This process should dampen the original CIEs, because on the meter scale, dissolution and re-precipitation of carbonate would involve δ^{13}C gradients in the DIC of surrounding pore water (Matter et al., 1977; Scholle and Arthur, 1980). This may explain, in part, why the magnitude of early Paleogene CIEs in bulk carbonate records are often muted relative to those found in other carbon-bearing phases (Slotnick et al., 2015b).

5.2 Oxygen isotopes and a problem recording past temperatures

The δ^{18}O record at Cicogna is intriguing because many of the CIEs are characterized by negative excursions but absolute values of δ^{18}O generally and unexpectedly increase upsection (Fig. 4). Similar results have been documented in bulk carbonate stable isotope records at other locations, such as ODP Site 1215 (Leon-Rodriguez and Dickens, 2010) and Mead Stream (Slotnick et al., 2012). Even the δ^{18}O record of bulk carbonate at ODP Site 1262 shows minimal long-term change from the late Paleocene to the early Eocene (Zachos et al., 2010), the time when high-latitude surface temperatures and deep ocean temperatures presumably increased by 5–6 °C, and one might expect a > 1 ‰ decrease in the δ^{18}O of marine carbonate.

Like previous workers, we cannot discount the notion that temperatures at low and high latitudes responded differently across the early Paleogene (Pearson et al., 2007; Huber and Caballero, 2011). Unlike for carbon isotopes, however, local dissolution and re-precipitation of carbonate should significantly impact the δ^{18}O of marine carbonate. This is because the oxygen water / rock ratio would be high before lithification, and because temperature strongly influences oxygen isotope fractionation (Matter et al., 1975; Scholle and Arthur, 1980; Frank et al., 1999). In general, as calcite-rich sediments and surrounding pore water are buried to higher temperatures along a geothermal gradient, local dissolution and re-precipitation of carbonate shifts carbonate δ^{18}O to lower values (above references; Schrag et al., 1995). It is likely that, during sediment burial, the bulk carbonate δ^{18}O records in many lower Paleogene sections, including at Cicogna, have been modified. We suggest that a signal of surface ocean temperature changes remains in the Cicogna section, which gives rise to short-term δ^{18}O excursions that coincide with CIEs and several known or suspected hyperthermal events. However, the entire δ^{18}O record at this location likely has shifted to more negative values preferentially with increasing burial depth and age. This partly explains the observed relationship between bulk carbonate δ^{13}C and δ^{18}O, which lies along a trajectory expected for diagenesis (Fig. 6). A potential test of this idea would be to show that the overgrowths on nannofossils (Plate I) have a significantly lower δ^{18}O than the primary core carbonate of nannofossil tests.
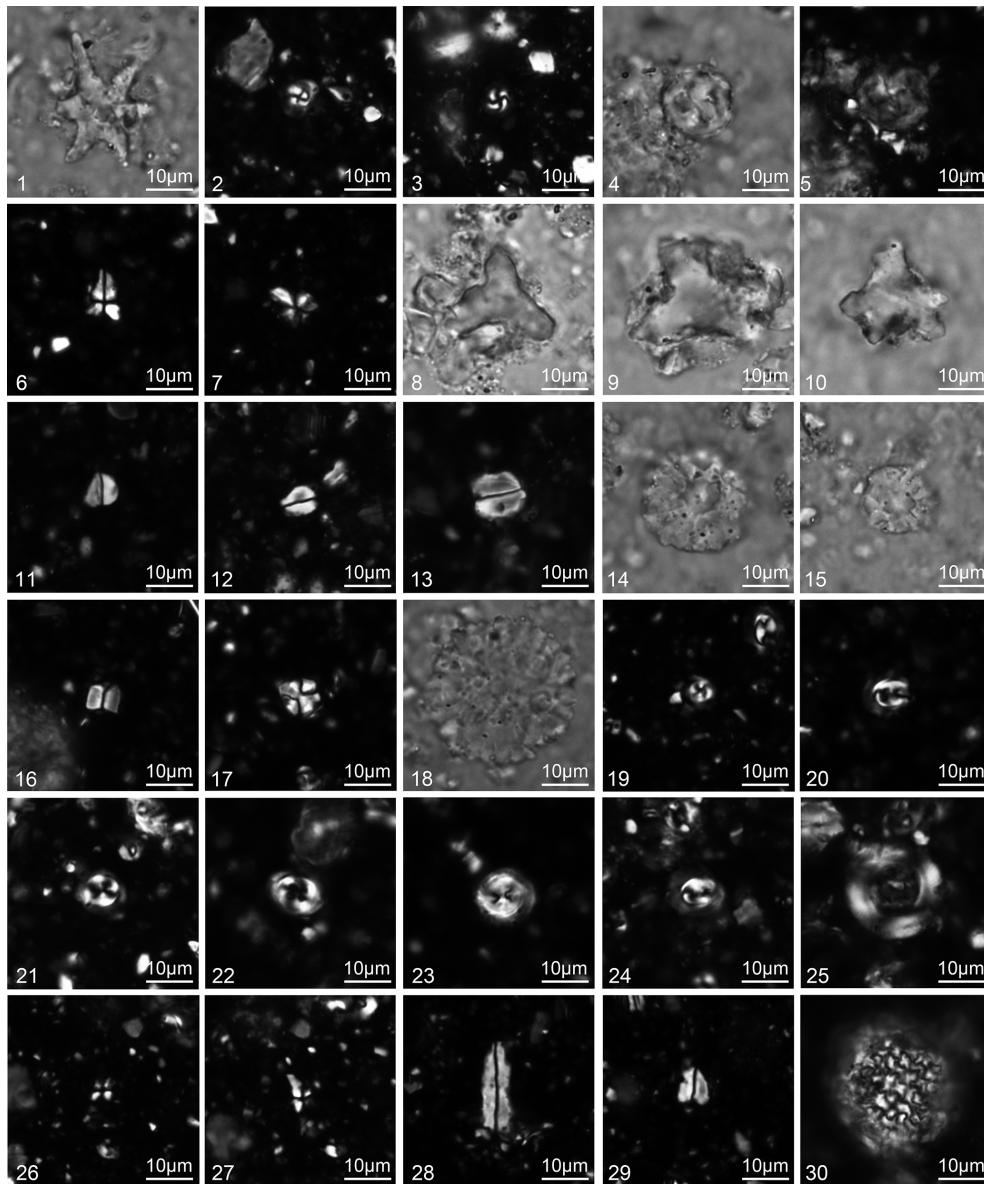
Plate 1. Images of selected calcareous nannofossil taxa from samples of the Cicogna section. Scale bar 10 µm. 1. *Discoaster lodoensis* (Bramlette and Riedel, 1954). Parallel light. Parallel nicols. Sample CIC/07-492. 2–3. *Girgisia gammation* (Bramlette and Sullivan, 1961; Varol, 1989). Crossed nicols. Sample CIC/07-437. 4–5. *Chiphragmalithus calathus* (Bramlette and Sullivan, 1961): 4, parallel light; 5, crossed nicols. Sample CIC/07-447. 6–7. *Sphenolithus radians* (Deflandre in Grassé, 1952): 6, crossed nicols 0°; 7, crossed nicols 45°. Sample CIC/07-437. 8. *Tribrachiatus orthostylus* (Shamrai, 1963). Parallel light. Sample 208-1262A-11H- 1, 149. Sample CIC/07-447. 9–10. *Tribrachiatus contortus* (Stradner, 1958; Bukry, 1972). Parallel light. Sample CIC/07-335. 11–13. *Zyghrablithus bijugatus* (Deflandre in Deflandre and Fert, 1954; Deflandre, 1959). Crossed nicols. Sample CIC/07-437. 14. *Discoaster salisburgensis* (Stradner, 1961). Parallel light. Sample CIC/07-335. 15. *Discoaster diastypus* (Bramlette and Sullivan, 1961). Parallel light. Sample CIC/07-335. 16. *Fasciculithus tympaniformis* (Hay and Mohler in Hay et al., 1967). Crossed nicols. Sample CIC/07-335. 17. *Octolithus multiplus* (Perch-Nielsen, 1973; Romein, 1979). Crossed nicols. Sample CIC/07-122. 18. *Discoaster multiradiatus* (Bramlette and Riedel, 1954). Parallel light. Sample CIC/07-122. 19. *Toweius pertusus* (Sullivan, 1965; Romein, 1979). Crossed nicols. Sample CIC/07-122. 20. *Toweius occultatus* (Locker, 1967; Perch-Nielsen, 1971). Crossed nicols. Sample CIC/07-122. 21. *Toweius eminens* (Bramlette and Sullivan, 1961; Perch-Nielsen, 1971). Crossed nicols. Sample CIC/07-029. 22. *Toweius eminens* (Bramlette and Sullivan, 1961; Perch-Nielsen, 1971). Crossed nicols. Sample CIC/07-029. 23. *Toweius eminens* (Bramlette and Sullivan, 1961; Perch-Nielsen, 1971). Crossed nicols. Sample CIC/07-122. 24. *Prinsius bisulcus* (Stradner, 1963; Hay and Mohler, 1967). Crossed nicols. Sample CIC/07-029. 25. *Ericsonia robusta* (Bramlette and Sullivan, 1961). Crossed nicols. Sample CIC/07-029. 26–27. *Sphenolithus anarrhopus* (Bukry and Bramlette, 1969): 26, crossed nicols 0°; 27, crossed nicols 45°. Sample CIC/07-029. 28–29. *Zyghrablithus bijugatus* (Deflandre in Deflandre and Fert, 1954; Deflandre, 1959). Crossed nicols. Sample CIC/07-122. 30. *Thoracosphaera saxea* (Stradner, 1961). Crossed nicols. Sample CIC/07-122.

5.3 Calcareous nannofossil assemblages within the context of correlative stable isotope records

A detailed stable carbon isotope curve provides a powerful tool to place past changes in calcareous nannofossil assemblages into a highly resolved framework. This is because, as implied above, truly global changes in the $\delta^{13}C$ composition of the ocean should occur within the cycling time of carbon through ocean, which is < 2000 years at present day and presumably for the entire Cenozoic (Broecker and Peng, 1982; Shackleton, 1986; Dickens et al., 1997).

Across the study interval at Cicogna, several calcareous nannofossil taxa appear or disappear (Table 1). Moreover, their abundances also change between these horizons (Figs. 7–9). One might hypothesize that these changes in nannofossil assemblages were related to the established (e.g., the PETM, H1/ETM-2 and K/X) and potential (e.g., the B1/B2, I1/I2) hyperthermal events that occurred during the late Paleocene and early Eocene (Figs. 1, 5). However, the timing between recorded evolutionary appearances and extinctions of calcareous nannofossils and perturbations in $\delta^{13}C$ is variable (Figs. 7–9). For instance, several significant calcareous nannofossil changes observed close to H1/H2 hyperthermals (e.g., B *T. othostylus*, B *S. radians*, B *S. villae*, Tc *D. multiradiatus*, T *T. contortus*) predate these events. By contrast, several biotic changes observed close to the B1/B2 CIEs (e.g., B *D. delicatus*, Tc *S. anarrhopus*, B *D. multiradiatus*, T *Ericsonia robusta*) happened at the end of these events. The PETM seems to provide the only case when a negative CIE precisely corresponds to major changes in calcareous nannofossil assemblages.

Profound changes in calcareous nannofossil assemblages occurred across the PETM in several locations (Fig. 2), both in terms of relative abundances and increases in origination and extinction rates (Aubry, 1998; Bown et al., 2004; Raffi et al., 2005; Gibbs et al., 2006a; Agnini et al., 2007a; Self-Trail et al., 2012). At Cicogna, the assemblages show remarkable, though mostly transient, relative abundance variations across the PETM, including an increase in *Coccolithus*, a decrease in *Zygrhablithus*, *Sphenolithus*, *Toweius* and *Prinsius*, and an extinction of most fasciculith species (Fig. 8). Not surprisingly, these changes are very similar to those in the Forada section, which is also located in the Belluno Basin (Agnini et al., 2007a).

Although these changes in relative abundance of taxa alone represent a notable difference with respect to background conditions, most of the changes are transient and/or local when compared with other data sets (Bralower, 2002; Gibbs et al., 2006b; Agnini et al., 2007b; Angori et al., 2007; Mutterlose et al., 2007). For instance, an increase in abundance of *Discoaster* and *Fasciculithus* was reported for some of the PETM section studied (e.g., Bralower, 2002; Tremolada and Bralower, 2004; Raffi et al., 2009), but these assemblage variations were not observed in other sections (e.g., Gibbs et al., 2006; Agnini et al., 2007a; Self-Trail et al.,

2012). The only global calcareous nannofossil assemblage features of the PETM are represented by the evolutionary appearance of *Rhomboaster/Tribrachiatus* lineage, the presence during the CIE of short-lived species such as *Discoaster araneus*, and the disappearance of several species of fasciculiths (Raffi et al., 2005; Agnini et al., 2007a).

While changes in calcareous nannoplankton assemblages during the PETM have been investigated at high resolution at different locations (e.g., Bralower, 2002; Gibbs et al., 2006b; Agnini et al., 2007a), the longer-term perspective in which such changes occurred during the early Paleogene has remained uncertain (Gibbs et al., 2012). The record at Cicogna provides this opportunity.

The PCA of calcareous nannofossil census data (%) indicates that two principal components (PC1 and PC2) account for most (56.0 %) of the variability in our 15 selected subgroups. Such analysis also permits the studied samples to be subdivided into two populations and a possible widely dispersed group (Fig. 10a). The first two populations are distinguished because of a major difference along the x axis representing PC1, whereas the third population seems to stand out because of a difference along the y axis representing PC2. Importantly, each of these three populations constitutes a homogeneous group in the time domain: group 1 includes all upper Paleocene samples (Paleocene samples and B1/B2 events); group 2 consists of almost all lower Eocene samples (Eocene samples, H1/H2 events and K event); and group 3 comprises samples that span the PETM (both core and recovery), and two samples that come from sediment deposited during the core of the H1 and B2 events (Fig. 10). These results indicate that late Paleocene calcareous nannofossil assemblages are statistically different in their composition from those of early Eocene samples. To check whether calcareous nannofossil assemblages across the PETM are statistically different from those of either the late Paleocene or the early Eocene, we performed MANOVA, which pointed out that ellipses containing 95 % of the data points for each group (late Paleocene, early Eocene and PETM) are virtually not overlapping one to each other, suggesting that three statistically different populations are recognized across the PETM, the late Paleocene and the early Eocene background assemblages, and the PETM fossil associations.

The general shift in the relative abundance of placoliths (i.e., *Coccolithus*, *Toweius* and *Prinsius*), the major component of the late Paleocene assemblages, to nannoliths/holococcoliths (i.e., *Sphenolithus* and *Zygrhablithus*), the major component of the early Eocene assemblages, largely explains the PC1 component or axis 1 (Fig. 10). By contrast, the dramatic shift toward negative values in the PC2 component or axis 2 during the PETM happens because of the increase in *Ericsonia* and reworking and the presence of *Rhomboaster–Tribrachiatus* plexus. Presumably, this relates to peculiar paleoenviromental conditions that developed during the event. One can hypothesize that this may have been a major difference in the physicochemical parameters of sea

surface waters, such as higher temperatures, higher nutrient concentration or reduced carbonate saturation state.

Statistical analysis of our data from Cicogna does not highlight any prominent short-term changes in calcareous nannofossil assemblages, other than across the PETM and perhaps the B2 and H1 events. However, several biohorizons occur around the B1/B2 events. Specifically, these are the Bc *Z. bijugatus*, the brief high abundance of *Octolithus* spp., the evolutionary onset of the *D. delicatus/D. multiradiatus* lineage, the presence of the short-ranged *E. robusta*, the final radiation of late Paleocene fasciculiths (i.e., *F. richardii* group, *F. hayi*, *F. lilianae*, *F. alanii*), and the Tc of *S. anarrhopus*. All these happened at Cicogna and at ODP Site 1262 within Chron C25n (Agnini et al., 2007b; Dallanave et al., 2009; Fig. 11), which spanned only 0.54 Myr (Westerhold et al., 2008). These near-synchronous events are intriguing because while the various nannofossils represent only minor components of late Paleogene assemblages, they were destined to become either an abundant constituent of Eocene populations (e.g., *Z. bijugatus* and the *D. delicatus/D. multiradiatus* lineage) or extinct after having been a distinctive element of Paleocene assemblages (e.g., *Fasciculithus* spp. and *S. anarrhopus)*. Following the PCIM, the long-term increase in temperature and decrease in δ^{13}C (Fig. 1) coincided with a series of minor changes in nannofossil assemblages, which subsequently became important, presumably for evolutionary reasons.

Similar to the late Paleocene, calcareous nannofossil assemblages after the PETM do not show major rearrangements of common taxa during the early Eocene. Instead, minor components of these assemblages exhibit a sequence of closely spaced biohorizons. The sequence of these biohorizons is T *Fasciculithus*, B *D. diastypus*, B *T. contortus*, T *T. bramlettei*, Tc *D. multiradiatus*, T *T. contortus*, B *T. orthostylus*, B *S. radians*, T *D. multiradiatus*, B *D. lodoensis*, B *G. gammation* and Bc *D. lodoensis* (Table 1). Within the resolution of available paleomagnetic and δ^{13}C data, all these biohorizons are virtually synchronous between the Cicogna section and ODP Site 1262 (Fig. 11). They also almost all occurred in near synchrony at DSDP Site 577 (Dickens and Backman, 2013), although the precise correlation remains uncertain, given problems with coring disturbance and subtleties in age models at this location.

Importantly, for stratigraphic purposes, the B and Bc of *D. lodoensis* are approximately coeval at all three locations and spaced apart by about 750 kyr. Unless one examines samples in detail, these two biohorizons can be confused and result in an erroneous assignment of early Eocene ages.

The evolutionary appearances and extinctions amongst early Eocene nannofossil assemblages may suggest the presence of uneven communities living in an extreme climate in which alterations of environmental conditions, even minor, might trigger evolutionary changes or prominent variations in abundances of a limited number of taxa that typically do not represent the dominant component of assemblages. A possible explanation is a generally higher tolerance of cosmopolitan taxa to variations in environmental conditions (Boucot, 1975; Winter et al., 1994). In contrast, highly specialized taxa that are adapted to a particular ecological niche may display greater sensitivity to modifications in the photic zone environment (MacArthur and Wilson, 1967; Pianka, 1970; Baumann et al., 2005).

In summary, several genera of calcareous nannofossils, such as *Rhomboaster*, *Tribrachiatus*, *Sphenolithus*, *Discoaster* and *Zygrhablithus* were, at least to some extent, affected during the late Paleocene–early Eocene transition, because they show an increased rate of taxonomic evolution (Fig. 11). However, these genera are all minor groups in terms of overall abundance, at least in most lower Paleogene sediment sequences, and they all belong to nannoliths and holococcoliths. It appears that these organisms were more sensitive to environmental changes than heterococcoliths, for example the cosmopolitan genera *Coccolithus* and *Toweius*.

5.4   Early Paleogene calcareous nannofossil evolution

Any comprehensive paleoenvironmental interpretation involving early Paleogene calcareous nannofossils remains tentative because many taxa, such as *Rhomboaster/Tribrachiatus*, *Discoaster*, *Sphenolithus* and *Zygrhablithus*, are extinct. Still, some single species or species groups are considered to be useful for reconstructions of paleoenvironmental conditions (Geisen et al., 2004). With that viewpoint, and with an understanding of modern holococcolith/nannolith ecology and classical biogeographical model, we provide a scenario regarding late Paleocene–early Eocene calcareous nannofossil evolution.

Modern holococcolithophores have numerous tiny rhombohedral calcite crystallites, and are considered as haploid stages of certain heterococcolithophores, which can live in just about any marine photic zone environment, although higher abundances and diversity are typical in oligotrophic settings (Billard and Inouye, 2004). The most common Paleogene holococcolith was *Zygrhablithus bijugatus*. This taxon has been interpreted as a *K* specialist more adapted to stable environments and oligotrophic conditions (Aubry, 1998; Bralower, 2002; Tremolada and Bralower, 2004; Agnini et al., 2007a; Self-Trail et al., 2012). Nannolith is a term used to describe peculiar morphotypes usually observed in association with coccoliths but lacking the typical features of heterococcoliths or holococcoliths. *Ceratolithus cristatus*, a modern nannolith, has been observed on the same cell together with *Neosphaera coccolithomorpha* (Alcolber and Jordan, 1997), suggesting that the nannolith stage (*C. cristatus*) corresponds to the holococcolith stage in other taxa (Young et al., 2005). Paleogene nannoliths include taxa with peculiar morphologies such as *Discoaster*, *Fasciculithus* and *Sphenolithus*. These genera often have been associated with warm waters and oligotrophic environments and are almost unanimously interpreted as *K* specialists (Haq and Lohmann,

1976; Backman, 1986; Wei and Wise, 1990; Bralower, 2002; Gibbs et al., 2004; 2006a, b; Agnini et al., 2007a). K specialists fluctuate at or near the carrying capacity (K) of the environment in which they thrive (MacArthur and Wilson, 1967), and are usually characterized by long individual life cycles and low reproductive potential. The K-specialist strategy is advantageous in highly stable, typically oligotrophic environments, which allows the evolution of stenotopy and where organisms compete by specialization and habitat partitioning (Hallock, 1987; Premoli Silva and Sliter, 1999). The narrow range of adaptability to changes in habitat or ecological conditions stimulates a rapid speciation.

At present, it is commonly accepted that modern holococcoliths and nannoliths are not produced by autonomous organisms; rather, they are stages in the life cycle of coccolithophores. Moreover, the passage between the two stages may be triggered by environmental factors (Billard and Inouye, 2004).

Hence, though Paleogene holococcoliths/nannoliths have no direct descendants in present-day oceans, they may very well have shared similar physiological features and life cycles with modern taxa. Assuming this is the case, the increase in the relative abundance of holococcoliths and nannoliths at the expense of heterococcoliths as well as the higher rates of evolution shown by holococcoliths and nannoliths may suggest conditions in which highly specialized taxa could flourish and rapidly evolve. This scenario is consistent with the idea, based on laboratory and modern ocean data, that the calcareous nannoplankton response to environmental change is species- or group-specific rather than homogeneous across the entire assemblage (Riebesell et al., 2000; Langer et al., 2006; Iglesias-Rodriguez et al., 2008; Lohbeck et al., 2012). Variations in the thermal and chemical structure of photic zone waters may thus account for the observed changes in the early Paleogene calcareous nannofossil assemblages.

5.5 Carbon isotope of surface waters during the early Paleogene

Like at Cicogna, well-preserved calcareous nannofossils dominate bulk sediment carbonate contents of early Paleogene strata at sites 577 and 1262 (Backman, 1986; Zachos et al., 2004; Dickens and Backman, 2013). Given that the nannofossil assemblages are fairly similar (Fig. 11), a very basic question returns: why is the overall early Paleogene bulk carbonate δ^{13}C record at Cicogna less by approximately 1 ‰?

A variety of explanations for the δ^{13}C offset can be offered. For example, sediments at Cicogna had greater amounts of organic matter, and during burial diagenesis, a fraction of this carbon was consistently added so as to decrease the δ^{13}C of pore water DIC. We note, though, that C_{org} contents (wt %) at the proximal Forada section generally have values less than 0.1 wt % (Giusberti et al., 2007). Similar C_{org} contents are found at ODP Site 1262, where values range from 0.0 to 0.3 wt % (Zachos et al., 2004).

A cursory examination of early Paleogene bulk carbonate δ^{13}C records from other sites of the North Atlantic/western Tethys region (e.g., sites 550 and 1051; Fig. 2) shows a commonality: these locations also display negative 0.5 to 1 ‰ offsets relative to correlative records at sites 577 and 1262 (Cramer et al., 2003). The δ^{13}C of DIC in modern surface waters (< 100 m) ranges by about 2 ‰, because of the differences in temperature, primary productivity and water mass mixing (Kroopnick, 1985; Tagliabue and Bopp, 2008). Notably, however, gradients in δ^{13}C of surface water DIC are gradual, such that large regions have fairly similar values. It is possible that bulk carbonate δ^{13}C values in early Paleogene North Atlantic sections record lower values than locations near the Equator or in southern latitudes because of past ocean circulation.

6 Summary and conclusions

We generate records of bulk carbonate δ^{13}C and δ^{18}O, $CaCO_3$ content and calcareous nannofossil assemblages from the Cicogna section, a marine sedimentary succession that now crops out along a stream in the Southern Alps of northeast Italy. The combined geochemical and calcareous nannofossil results allow us to generate a detailed stratigraphy for the section, as well as to explore relationships between stable isotope variations and nannofossil assemblages. Most lower Paleogene sections examined to date lack such coupled data sets.

The δ^{13}C record and calcareous nannofossil assemblages show that the section spans ~ 5.3 Myr of the late Paleocene and early Eocene interval, from 57.5 to 52.2 Ma on the WO-1 timescale. This is consistent with previous paleomagnetic information and preliminary calcareous nannofossil biostratigraphy (Dallanave et al., 2009), but provides a more detailed stratigraphic framework, one appropriate for correlations to other locations around the world. In particular, the fairly well resolved δ^{13}C record shows long-term and short variations that correspond to those found in several other sections, including an established series of negative CIEs. The most prominent CIE marks the PETM, while other less pronounced CIEs represent the H-1, K/X and other "events" documented elsewhere. The δ^{13}C variations observed at Cicogna clearly reflect global changes in the fluxes of carbon to and from the ocean and atmosphere.

PCA of calcareous nannofossil assemblages shows three distinct sample clusters. Late Paleocene and early Eocene assemblages were distinctly different from each other and from that of the PETM. Indeed, the PETM, the most intense hyperthermal during the late Paleocene–early Eocene, was characterized by a unique calcareous nannofossil assemblage composition. This suggests that the brief episode of extreme warming permanently modified the composition of calcareous nannoplankton through an increase in the rate of taxonomic evolution (Gibbs et al., 2006a). Less prominent hy-

perthermal events do not show significant variations in the main components of assemblages but rather were characterized by a series of changes affecting a limited number of rare taxa. These taxa may have been less tolerant to environmental changes in their habitats.

More common taxa, essentially consisting of placoliths, such as the cosmopolitan *Coccolithus* and *Toweius*, display a progressive long-term decrease interrupted by transient changes in their relative abundance but virtually no extinction or origination events occur in these groups during the pertinent time interval. Species belonging to nannoliths and holococcoliths (*Discoaster*, *Fasciculithus*, *Rhomboaster/Tribrachiatus*, *Sphenolithus* and *Zygrhablithus*), generally show a higher rate of evolution and a higher concentration of biohorizons close to δ^{13}C perturbations. In conclusion, calcareous nannoplankton show a different response of the various components of the assemblages; this is consistent with a species or taxonomic unit sensitivity of calcareous phytoplankton to paleoenviromental perturbations. This evolutionary climate-forced model is supported by data from ODP Site 1262, which demonstrate that these changes are global and synchronous between middle latitudes in the western Tethys region and the South Atlantic.

The Supplement related to this article is available online at doi:10.5194/cp-12-883-2016-supplement.

References

Adelseck Jr., C. G., Geehan, G. W., and Roth, P. H.: Experimental evidence for the selective dissolution and overgrowth of calcareous nannofossils during diagenesis, Geol. Soc. Am. Bull., 84, 2755–2762, 1973.

Agnini, C., Muttoni, G., Kent, D. V., and Rio, D.: Eocene biostratigraphy and magnetic stratigraphy from Possagno, Italy: The calcareous nannofossil response to climate variability, Earth Planet. Sc. Lett., 241, 815–830, doi:10.1016/j.epsl.2005.11.005, 2006.

Agnini, C., Fornaciari, E., Rio, D., Tateo, F., Backman, J., and Giusberti, L.: Responses of calcareous nannofossil assemblages, mineralogy and geochemistry to the environmental perturbations across the Paleocene/Eocene boundary in the Venetian Pre–Alps, Mar. Micropaleontol., 63, 19–38, doi:10.1016/j.marmicro.2006.10.002, 2007a.

Agnini, C., Fornaciari, E., Raffi, I., Rio, D., Röhl, U., and Westerhold, T.: High-resolution nannofossil biochronology of middle Paleocene to early Eocene at ODP Site 1262: implications for calcareous nannoplankton evolution, Mar. Micropaleontol., 64, 215–248, doi:10.1016/j.marmicro.2007.05.003, 2007b.

Agnini, C., Macrì, P., Backman, J., Brinkhuis, H., Fornaciari, E., Giusberti, L., Luciani, V., Rio, D., Sluijs, A., and Speranza, F.: An early Eocene carbon cycle perturbation at 52.5 Ma in the Southern Alps: Chronology and biotic response, Paleoceanography, 24, PA2209, doi:10.1029/2008PA001649, 2009.

Agnini, C., Fornaciari, E., Giusberti, L., Grandesso, P., Lanci, L., Luciani, V., Muttoni, G., Pälike, H., Rio, D., Spofforth, D. J. A., and Stefani, C.: Integrated bio-magnetostratigraphy of the Alano section (NE Italy): a proposal for defining the middle-late Eocene boundary, Geol. Soc. Am. Bull., 123, 841–872, doi:10.1130/B30158.1, 2011.

Agnini, C., Fornaciari, E., Raffi, I., Catanzariti, R., Pälike, H., Backman, J., and Rio, D.: Biozonation and biochronology of Paleogene calcareous nannofossils from low and middle latitudes, Newslett. Stratigr., 47, 131–181, doi:10.1127/0078-0421/2014/0042, 2014.

Aitchison, J.: The Statistical Analysis of Compositional Data, Chapman and Hall, London – New York, 12, 1–416, 1986.

Alcober, J. A. and Jordan, R. W.: An interesting association between *Neosphaera coccolithomorpha* and *Ceratolithus cristatus*, Eur. J. Phycol., 32, 91–93, 1997.

Angori, E., Bernaola, G., and Monechi, S.: Calcareous nannofossil assemblages and their response to the Paleocene-Eocene Thermal Maximum event at different latitudes: ODP Site 690 and Tethyan sections, Geol. S. Am. S., 424, 69–85, doi:10.1130/2007.2424(04), 2007.

Aubry, M.-P.: Handbook of Cenozoic Calcareous Nannoplankton, book 1, Ortholithae (Discoaster), Am. Mus. Nat. Hist. Micropaleontol. Press, New York, 1–263, 1984.

Aubry, M.-P.: Handbook of Cenozoic Calcareous Nannoplankton, book 2, Ortholithae (Holococcoliths, Ceratoliths, Ortholiths and Other), Am. Mus. Nat. Hist. Micropaleontol. Press, New York, 1–279, 1988.

Aubry, M.-P.: Handbook of Cenozoic Calcareous Nannoplankton, book 3, Ortholithae (Pentaliths and Other), Heliolithae (Fasciculiths, Sphenoliths and Other), Am. Mus. Nat. Hist. Micropaleontol. Press, New York, 1–279, 1989.

Aubry, M.-P.: Handbook of Cenozoic Calcareous Nannoplankton, book 4, Heliolithae (Helicoliths, Cribriliths, Lopadoliths and Other), Am. Mus. Nat. Hist. Micropaleontol. Press, New York, 1–381, 1990.

Aubry, M.-P.: Early Paleogene calcareous nannoplankton evolution: a tale of climatic amelioration, in: Late Paleocene–early Eocene Biotic and Climatic Events in the Marine and Terrestrial Records, Columbia University Press, New York, 158–201, 1998.

Aubry, M.-P.: Late Paleocene–early Eocene sedimentary history in western Cuba: implications for the LPTM and for regional tectonic history, Micropaleontol., 45, 5–18, 1999a.

Aubry, M.-P.: Handbook of Cenozoic Calcareous Nannoplankton, book 5, Heliolithae (Zygoliths and Rhabdoliths), Am. Mus. Nat. Hist. Micropaleontol. Press, New York, 1–368, 1999b.

Aubry, M.-P. and Salem, R.: The Dababiya Core: A window into Paleocene to early Eocene depositional history in Egypt based on coccolith stratigraphy, Stratigraphy, 9, 287–346, 2012.

Baccelle, L. and Bosellini, A.: Diagrammi per la stima visiva della composizione percentuale nelle rocce sedimentary, Ann. Univ. Ferrara, 9, 59–62, 1965.

Backman, J.: Late Paleocene to middle Eocene calcareous nannofossil biochronology from the Shatsky Rise, Walvis Ridge and Italy, Palaeogeogr. Palaeocl., 57, 43–59, 1986.

Backman, J. and Shackleton N. J.: Quantitative biochronology of Pliocene and early Pleistocene calcareous nannoplankton from the Atlantic, Indian and Pacific Oceans, Mar. Micropaleontol., 8, 141–170, doi:10.1016/0377-8398(83)90009-9, 1983.

Baumann, K.-H., Andruleit, H., Böckel, B., Geisen, M., and Kinkel, H.: The significance of extant coccolithophores as indicators of ocean water masses, surface water temperature, and palaeoproductivity: a review, Paläontol. Zeitsch., 79, 93–112, 2005.

Bernoulli, D. and Jenkyns, H. C.: Alpine, Mediterranean, and Central Atlantic Mesozoic facies in relation to the early evolution of the Tethys, in: Modern and Ancient Geosynclinal Sedimentation, Society for Sedimentary Geology (SEPM) Special Publication, 19, 19–160, 1974.

Bernoulli, D., Caron, C., Homewood, P., Kalin, O., and Van Stuijvenberg, J.: Evolution of continental margins in the Alps, Schweiz, Miner. Petrol., 59, 165–170, 1979.

Bijl, P. K., Schouten, S., Sluijs, A., Reichart, G. J., Zachos, J. C., Brinkhuis, H.: Early Palaeogene temperature evolution of the southwest Pacific Ocean, Nature, 461, 776–779, doi:10.1038/nature08399, 2009.

Billard, C. and Innouye, I.: What is new in coccolithophore biology?, in: Coccolithophores – From Molecular Processes to Global Impact, Springer, Berlin, 1–29, 2004.

Bordiga, M., Henderiks, J., Tori, F., Monechi, S., Fenero, R., Legarda-Lisarri, A., and Thomas, E.: Microfossil evidence for trophic changes during the Eocene-Oligocene transition in the South Atlantic (ODP Site 1263, Walvis Ridge), Clim. Past, 11, 1249–1270, doi:10.5194/cp-11-1249-2015, 2015.

Bornemann, A. and Mutterlose, J.: Calcareous nannofossil and δ^{13}C records from the Early Cretaceous of the Western Atlantic Ocean: evidence for enhanced fertilization across the Berriasian–Valanginian transition, Palaios, 23, 821–832, 2008.

Boucot, A. J.: Evolution and Extinction Rate Controls, Elsevier, Amsterdam, the Netherlands, 250 pp., 1975.

Bown, P. R.: Paleogene calcareous nannofossils from the Kilwa and Lindi areas of coastal Tanzania: Tanzania Drilling Project Sites 1 to 10, J. Nannoplankt. Res., 27, 21–95, 2005.

Bown, P. and Pearson, P.: Calcareous plankton evolution and the Paleocene/Eocene thermal maximum event: New evidence from Tanzania, Mar. Micropaleontol., 71, 60–70, doi:10.1016/j.marmicro.2009.01.005, 2009.

Bown, P. R. and Young, J. R.: Techniques, in: Calcareous Nannofossil Biostratigraphy, Chapman & Hall, London, 16–28, 1998.

Bown, P. R., Lees, J. A., and Young, J. R.: Calcareous nannoplankton evolution and diversity through time, in: Coccolithophores – From Molecular Processes to Global Impact, Springer, Berlin, 481–508, 2004.

Bralower, T. J.: Evidence of surface water oligotrophy during the Paleocene–Eocene thermal maximum: nannofossil assemblage data from Ocean Drilling Program Site 690,

Maud Rise, Weddell Sea, Paleoceanography, 17, 1029–1042, doi:10.1029/2001PA000662, 2002.

Bralower, T. J. and Mutterlose, J.: Calcareous nannofossil biostratigraphy of ODP Site 865, Allison Guyot, Central Pacific Ocean: a tropical Paleogene reference section, Proc. Ocean. Drill. Prog. Sci. Results, 143, 31–72, doi:10.2973/odp.proc.sr.143.204.1995, 1995.

Bramlette, M. N. and Riedel, W. R.: Stratigraphic value of discoasters and some other microfossils related to Recent coccolithophores, J. Paleontol., 28, 385–403, 1954.

Bramlette, M. N. and Sullivan, F. R.: Coccolithophorids and related nannoplankton of the Early Tertiary in California, Micropaleontol., 7, 129–188, 1961.

Broecker, W. S. and Peng, T.-H.: Tracers in the Sea, Eldigio Press, LamontDoherty Geological Observatory, Palisades, New York, 1–690, 1982.

Buccianti, A., Mateu-Figueras, G., and Pawlowsky-Glahn, V.: Compositional data analysis in the geosciences: From theory to practice, Geol. Soc. London, London, Spec. Publ., 264, 1–206, doi:10.1144/GSL.SP.2006.264.01.16, 2006.

Bukry, D.: Further comments on coccolith stratigraphy, Leg 12 Deep Sea Drilling Project, Proc. DSDP, Init. Repts, 12, 1071–1083, 1972.

Bukry, D.: Low-latitude coccolith biostratigraphic zonation, Initial Rep. Deep Sea, 15, 685–703, 1973.

Bukry, D. and Bramlette, M. N.: Some new and stratigraphically useful calcareous nannofossils of the Cenozoic, Tulane Studies in Geology, 7, 13–142, 1969.

Cande, S. C. and Kent, D. V.: Revised calibration of the geomagnetic polarity timescale for the Late Cretaceous and Cenozoic, 100, 6093–6096, doi:10.1029/94JB03098, 1995.

Cati, A., Sartorio, D., and Venturini, S.: Carbonate platforms in the subsurface of the northern Adriatic area, Mem. Soc. Geol. It., 40, 295–308, 1989.

Corfield, R. M.: Palaeocene oceans and climate: An isotopic perspective, Earth Sci. Rev., 37, 225–252, doi:10.1016/0012-8252(94)90030-2, 1994.

Costa, V., Doglioni, C., Grandesso, P., Masetti, D., Pellegrini, G. B., and Tracanella, E.: Carta Geologica d'Italia, Foglio 063, Belluno: Roma, Servizio Geologico d'Italia, scale 1 : 50 000, 74 pp., 1996.

Cramer, B. S., Wright, J. D., Kent, D. V., and Aubry, M.-P.: Orbital climate forcing of δ^{13}C excursions in the late Paleocene–early Eocene (Chrons C24n–C25n), Paleoceanography, 18, 1097, doi:10.1029/2003PA000909, 2003.

Cramer, B. S., Toggweiler, J. R., Wright, J. D., Katz, M. E., and Miller, K. G.: Ocean overturning since the Late Cretaceous: Inferences from a new benthic foraminiferal isotope compilation, Paleoceanogaphy, 24, PA4216, doi:10.1029/2008PA001683, 2009.

Dallanave, E., Agnini, C., Muttoni, G., and Rio, D.: Magnetobiostratigraphy of the Cicogna section (Italy): implications for the late Paleocene-early Eocene time scale, Earth Planet. Sc. Lett., 285, 39–51, doi:10.1016/j.epsl.2009.05.033, 2009.

Dallanave, E., Agnini, C., Bachtadse, V., Muttoni, G., Crampton, J. S., Strong, C. P., Hines, B. R., Hollis, C. J., and Slotnick., B. S.: Early to middle Eocene magnetostratigraphy of the southwest Pacific Ocean and climate influence on sedimentation: insights from the Mead Stream section, New Zealand, Geol. Soc. Am. Bull., 127, 643–660, doi:10.1130/B31147.1, 2015.

DeConto, R. M., Galeotti, S., Pagani, M., Tracy, D., Schaefer, K. Zhang, T., Pollard, D., and Beerling D. J.: Past extreme warming events linked to massive carbon release from thawing permafrost, Nature, 484, 87–91, doi:10.1038/nature10929, 2012.

Deflandre, G.: Classe des Coccolithophoridés, (Coccolithophoridae, Lohmann, 1902), in: Traite de Zoologie. Masson, Paris, 439–470, 1952.

Deflandre, G.: Sur les nannofossiles calcaires et leur systématique, Revue de Micropaleontologie, 2, 127–152, 1959.

Deflandre, G. and Fert, C.: Observations sur les coccolithophoridés actuels et fossiles en microscopie ordinaire et Électronique, Annales de Paléontologie, 40, 115–176, 1954.

Dickens, G. R.: Methane oxidation during the late Palaeocene thermal maximum, B. Soc. Geol. Fr., 171, 37–49, 2000.

Dickens, G. R.: Rethinking the global carbon cycle with a large, dynamic and microbially mediated gas hydrate capacitor, Earth Planet. Sc. Lett., 213, 169–183, 2003.

Dickens, G. R. and Backman, J.: Core alignment and composite depth scale for the lower Paleogene through uppermost Cretaceous interval at Deep Sea Drilling Project Site 577, Newslett. Stratigr., 46, 47–68, doi:10.1127/0078-0421/2013/0027, 2013.

Dickens, G. R., Castillo, M. M., and Walker, J. C. G.: A blast of gas in the latest Paleocene: Simulating first-order effects of massive dissociation of oceanic methane hydrate, Geology, 25, 259–262, 1997.

Doglioni, C. and Bosellini, A.: Eoalpine and mesoalpine tectonics in the Southern Alps, Geol. Rundsch., 77, 734–754, 1987.

Dupuis, C., Aubry, M.-P., Steurbaut, E., Berggren, W. A., Ouda, K., Magioncalda, R., Cramer, B. S., Kent, D. V., Speijer, R. P., and Heilmann-Clausen, C.: The Dababiya Quarry section: lithostratigraphy, geochemistry and paleontology, Micropaleontology, 49, 41–59, 2003.

Erba, E., Bottini, C., Weissert, H. J., and Keller, C. E.: Calcareous nannoplankton response to surface-water acidification around Oceanic Anoxic Event 1a, Science, 329, 428–432, doi:10.1126/science.1188886, 2010.

Frank, T. D., Arthur, M. A., and Dean W. E.: Diagenesis of Lower Cretaceous pelagic carbonates, North Atlantic: paleoceanographic signals obscured, J. Foramin. Res., 29, 340–351, 1999.

Galeotti, S., Krishnan, S., Pagani, M., Lanci, L., Gaudio, A., Zachos, J. C., Monechi, S., Morelli, G., and Lourens, L.: Orbital chronology of early Eocene hyperthermals from the Contessa Road section, central Italy, Earth Planet. Sc. Lett., 290, 192–200, doi:10.1016/j.epsl.2009.12.021, 2010.

Geisen, M., Young, J. R., Probert, I., Sáez, A. G., Baumann, K.-H., Bollmann, J., Cros, L., De Vargas, C., Medlin, L. K., and Sprengel, C.: Species level variation in coccolithophores, in: Coccolithophores – From Molecular Processes to Global Impact, Springer, Berlin, 327–366, 2004.

Gibbs, S. J., Shackleton, N. J., and Young, J. R.: Orbitally forced climate signals in mid-Pliocene nannofossil assemblages, Mar. Micropaleontol., 51, 39–56, 2004.

Gibbs, S. J., Bown, P. R., Sessa, J. A., Bralower, T. J., and Wilson, P. A.: Nannoplankton extinction and origination across the Paleocene-Eocene thermal maximum, Science, 314, 1770–1773, doi:10.1126/science.1133902, 2006a.

Gibbs, S. J., Bralower, T. J., Bown, P. R., Zachos, J. C., and Bybell, L. M.: Shelf and open-ocean calcareous phytoplankton assemblages across the Paleocene–Eocene thermal maximum: implications for global productivity gradients, Geology, 34, 233–236, doi:10.1130/G22381.1, 2006b.

Gibbs, S. J., Bown, P. R., Murphy, B. H., Sluijs, A., Edgar, K. M., Pälike, H., Bolton, C. T., and Zachos, J. C.: Scaled biotic disruption during early Eocene global warming events, Biogeosciences, 9, 4679–4688, doi:10.5194/bg-9-4679-2012, 2012.

Giusberti, L., Rio, D., Agnini, C., Backman, J., Fornaciari, E., Tateo, F., and Oddone, M.: Mode and tempo of the Paleocene-Eocene Thermal Maximum in an expanded section in the Venetian Pre-Alps, Geol. Soc. Am. Bull., 119, 391–412, doi:10.1130/B25994.1, 2007.

Giusberti, L., Boscolo Galazzo, F., and Thomas, E.: Variability in climate and productivity during the Paleocene-Eocene Thermal Maximum in the western Tethys (Forada section), Clim. Past, 12, 21–240, doi:10.5194/cp-12-213-2016, 2016.

Grandesso, P.: Biostratigrafia delle formazioni terziarie del Vallone Bellunese, B. Soc. Geol. Ital., 94, 1323–1348, 1976.

Hallock, P.: Fluctuations in the trophic resource continuum: A factor in global diversity cycles?, Paleoceanography, 2, 457–471, 1987.

Hammer, Ø, Harper, D. A. T., and Ryan, P. D.: PAST: Paleontological statistics software package for education and data analysis, Palaeontol. Electron., 4, 9 pp., 2001.

Haq, B. U. and Lohmann, G. P.: Early Cenozoic calcareous nannoplankton biogeography of the Atlantic Ocean, Mar. Micropaleontol., 1, 119–194, 1976.

Harris, A. D., Miller, K. G., Browning, J. V., Sugarman, P. J., Olsson, R. K., Cramer, B. S., and Wright, J. D.: Integrated stratigraphic studies of Paleocene – lowermost Eocene sequences, New Jersey Coastal Plain: Evidence for glacioeustatic control, Paleoceanography, 25, PA3211, doi:10.1029/2009PA001800, 2010.

Hay, W. W.: Carbonate fluxes and calcareous nannoplankton, in: Coccolithophores – From Molecular Processes to Global Impact, Springer, Berlin, 508–528, 2004.

Hay, W. W. and Mohler, H. P.: Calcareous nannoplankton from Early Tertiary rocks at Point Labau, France and Paleocene-Early Eocene correlations, J. Paleont., 41, 1505–1541, 1967.

Hay, W. W., Mohler, H. P., Roth, P. H., Schmidt, R. R., and Boudreaux, J. E.: Calcareous nannoplankton zonation of the Cenozoic of the Gulf Coast and Caribbean-Antillean area, and transoceanic correlation, Transactions of the Gulf Coast Association of Geological Societies, 17, 428–480, 1967.

Hollis, C. J., Taylor, K. W. R., Handley, L., Pancost, R. D., Huber, M., Creech, J. B., Hines, B.R., Crouch, E. M., Morgans, H. E. G., Crampton, J. S., Gibbs, S., Pearson, P. N., and Zachos, J. C.: Early Paleogene temperature history of the southwest Pacific Ocean: Reconciling proxies and models, Earth Planet. Sc. Lett., 349–350, 53–66, 2012.

Hönisch, B., Ridgwell, A., Schmidt, D. N., Thomas, E., Gibbs, S. J., Sluijs, A., Zeebe, R., Kump, L., Martindale, R. C., Greene, S. E., Kiessling, W., Ries, J., Zachos, J. C., Royer, D. L., Barker, S., Marchitto Jr., T. M., Moyer, R., Pelejero, C., Ziveri, P., Foster, G. L., and Williams, B.: The geological record of ocean acidification, Science, 335, 1058–1063, doi:10.1126/science.1208277, 2012.

Huber, M. and Caballero, R.: The early Eocene equable climate problem revisited, Clim. Past, 7, 603–633, doi:10.5194/cp-7-603-2011, 2011.

Iglesias-Rodriguez, M. D., Halloran, P. R., Rickaby, R. E. M., Hall, I. R., Colmenero-Hidalgo, E., Gittins, J. R., Green, D. R. H., Tyrrell, T., Gibbs, S. J., Von Dassow, P., Rehm, E., Armbrust, E. V., and Boessenkool, K. P.: Phytoplankton calcification in a high-CO_2 world, Science, 320, 336–340, doi:10.1126/science.1154122, 2008.

Jiang, S. and Wise Jr., S. W: Distinguishing the influence of diagenesis on the paleoecological reconstruction of nannoplankton across the Paleocene/Eocene Thermal Maximum: An example from the Kerguelen Plateau, southern Indian Ocean, Mar. Micropaleontol., 72, 49–59, doi:10.1016/j.marmicro.2009.03.003, 2009.

Keeling, C. D. and Whorf, T. P.: Atmospheric carbon dioxide record from Mauna Loa, in: Oak Ridge Laboratory Trends: A Compendium of Data on Global Change, Carbon Dioxide Information Analysis Center, Oak Ridge National Laboratory, US Department of Energy, Oak Ridge, Tennessee, USA, available at: http://cdiac.esd.ornl.gov/trends/co2/sio-keel-flask/sio-keel-flask.html (last access: 4 April 2015), 2004.

Kirtland-Turner, S., Sexton, P. F., Charles, C. D., and Norris, R. D.: Persistence of carbon release events through the peak of early Eocene global warmth, Nat. Geosci., 7, 748–751, doi:10.1038/ngeo2240, 2014.

Kleypas, J. A., Feely, R. A., Fabry, V. J., Langdon, C., Sabine, C. L., and Robbins, L. L.: Impacts of ocean acidification on coral reefs and other marine calcifiers: A guide for future research, Contrib. No. 2857, NOAA/Pacific Marine Environm. Lab., 88 pp., 2006.

Komar, N., Zeebe, R. E., and Dickens, G. R.: Understanding long-term carbon cycle trends: The late Paleocene through the early Eocene, Paleoceanography, 28, 650–662, doi:10.1002/palo.20060, 2013.

Krishnan, S., Pagani, M., and Agnini, C.: Leaf waxes as recorders of paleoclimatic changes during the Paleocene-Eocene Thermal Maximum: Regional expressions from the Belluno Basin, Org. Geochem., 80, 8–17, doi:10.1016/j.orggeochem.2014.12.005, 2015.

Kroopnick, P. M.: The distribution of ^{13}C of ΣCO_2 in the world oceans, Deep-Sea Res., 32, 57–84, 1985.

Kucera, M. and Malmgren, B. A.: Logratio transformation of compositional data – a resolution of the constant sum constraint, Mar. Micropaleontol., 34, 117–120, 1998.

Kump, L. R., Bralower, T. J., and Ridgwell, A.: Ocean acidification in deep time, Oceanography, 22, 94–107, 2009.

Kurtz, A. C., Kump, L. R., Arthur, M. A., Zachos, J. C., and Paytan, A.: Early Cenozoic decoupling of the global carbon and sulfur cycles, Paleoceanography, 18, 1090, doi:10.1029/2003PA000908, 2003.

Langer, G., M., Geisen, Baumann, K.-H., Kläs, J., Riebesell, U., Thoms, S., and Young, J. R.: Species-specific response of calcifying algae to changing seawater carbonate chemistry, Geochem. Geophy. Geosy., 7, Q09006, doi:10.1029/2005GC001227, 2006.

Leon-Rodriguez, L. and Dickens, G. R.: Constraints on ocean acidification associated with rapid and massive carbon injections: The early Paleogene record at Ocean Drilling Program Site 1215, Equatorial Pacific Ocean, Palaeogeogr. Palaeocl., 298, 409–420, doi:org/10.1016/j.palaeo.2010.10.029, 2010.

Locker, S.: Neue, statigraphisch wichtige Coccolithophoriden (Flagellata aus dem norddeutschen Altetiar, Monatsber. Deutsch. Akad. Wiss. Berlin, 9, 758–769, 1967.

Lohbeck, K. T., Riebesell, U., and Reusch, T. B. H.: Adaptive evolution of a key phytoplankton species to ocean acidification, Nat. Geosci., 5, 346–351, doi:10.1038/ngeo1441, 2012.

Lourens, L. J., Sluijs, A., Kroon, D., Zachos, J. C., Thomas, E., Röhl, U., Bowles, J., and Raffi, I.: Astronomical pacing of late Palaeocene to early Eocene global warming events, Nature, 435, 1083–1087, doi:10.1038/nature03814, 2005.

Lunt, D. J., Ridgwell, A., Sluijs, A., Zachos, J. C., Hunter, S., and Haywood, A.: A model for orbital pacing of methane hydrate destabilization during the Palaeogene, Nat. Geosci., 4, 775–778, doi:10.1038/ngeo1266, 2011.

MacArthur, R. and Wilson, E. O.: The Theory of Island Biogeography, Princeton University Press, ISBN 0-691-08836-5M, 1967.

Milliman, J. D.: Production and accumulation of calcium carbonate in the ocean: Budget of a nonsteady state, Global Biogeochem. Cy., 7, 927–957, doi:10.1029/93GB02524, 1993.

Marino, M., Maiorano, P., and Lirer, F.: Changes in calcareous nannofossil assemblages during the Mid-Pleistocene Revolution, Mar. Micropaleontol., 69, 70–90, doi:10.1016/j.marmicro.2007.11.010, 2008.

Martini, E.: Standard Tertiary and Quaternary calcareous nannoplankton zonation, in: Proceedings of the 2nd Planktonic Conference, 2, Tecnoscienza, Roma, 739–785, 1971.

Matter, A., Douglas, R. G., and Perch-Nielsen, K.: Fossil preservation, geochemistry and diagenesis of pelagic carbonates from Shatsky Rise, northwest Pacific, Init. Rep. DSDP, 32, 891–922, 1975.

Mixon, R. B. and Powars D. S.: Folds and faults in the inner Coastal Plain of Virginia and Maryland: their effect on the distribution and thickness of Tertiary rock units and local geomorphic history, in: Cretaceous and Tertiary Stratigraphy, paleontology, and structure, southwestern Maryland and northeastern Virginia, edited by: Frederiksen, N. O. and Kraft, K., American Association of Stratigraphic Palynologists Field Trip Volume and Guidebook (1984), 112–122, 1994.

Monechi, S., Angori, E., and von Salis, K.: Calcareous nannofossil turnover around the Paleocene/Eocene transition at Alamedilla (southern Spain), B. Soc. Geol. Fr., 171, 477–489, 2000.

Mutterlose, J., Linnert, C., and Norris, R.: Calcareous nannofossils from the Paleocene–Eocene Thermal Maximum of the equatorial Atlantic (ODP Site 1260B): Evidence for tropical warming, Mar. Micropaleontol., 65, 13–31, doi:10.1016/j.marmicro.2007.05.004, 2007.

Nicolo, M. J., Dickens, G. R., Hollis, C. J., and Zachos, J. C.: Multiple early Eocene hyperthermals: Their sedimentary expression on the New Zealand continental margin and in the deep sea, Geology, 35, 699–702, doi:10.1130/G23648A.1, 2007.

Norris, R. D., Wilson, P. A., Blum, P., and the Expedition 342 Scientists: Expedition 342 summary, Proc. IODP, 342, 1–149, doi:10.2204/iodp.proc.342.2014, 2014.

Ogg, J. G. and Bardot, L.: Aptian through Eocene magnetostratigraphic correlation of the Blake Nose Transect (Leg 171B), Florida continental margin, Proc. ODP, Sci. Results, 171B, 1–58, doi:10.2973/odp.proc.sr.171B.104.2001, 2001.

Ogg, J. and Smith, A.,: The geomagnetic polarity time scale, in: The Geologic Time Scale 2012, edited by: Gradstein, F. M., Ogg, J. G., and Schmitz, M. D., Amsterdam, the Netherlands, Elsevier, 63–86, 2004.

Ogg, J. and Smith, A.,: The geomagnetic polarity time scale, in: The Geologic Time Scale 2012, edited by: Gradstein, F. M., Ogg, J. G., Schmitz, M. D., and Ogg, G. M., Amsterdam, the Netherlands, Elsevier, 85–113, 2012.

Okada, H. and Bukry, D.: Supplementary modification and introduction of code numbers to the low-latitude coccolith biostratigraphic zonation (Bukry, 1973; 1975), Mar. Micropaleontol., 5, 321–325, doi:10.1016/0377-8398(80)90016-X, 1980.

Pälike, H., Lyle, M. W., Nishi, H., Raffi, I., Ridgwell, A., Gamage, K., Klaus, A., Acton, G. D., Anderson, L., Backman, J., Baldauf, J. G., Beltran, C., Bohaty, S. M., Bown, P. R., Busch, W. H., Channell, J. E. T., Chun, C. O. J., Delaney, M. L., Dewang, P., Dunkley Jones, T., Edgar, K. M., Evans, H. F., Fitch, P., Foster, G. L., Gussone, N., Hasegawa, H., Hathorne, E. C., Hayashi, H., Herrle, J. O., Holbourn, A. E. L., Hovan, S. A., Hyeong, K., Iijima, K., Ito, T., Kamikuri, S.-I., Kimoto, K., Kuroda, J., Leon-Rodriguez, L., Malinverno, A., Moore, T. C., Murphy, B., Murphy, D. P., Nakamura, H., Ogane, K., Ohneiser, C., Richter, C., Robinson, R. S., Rohling, E. J., Romero, O. E., Sawada, K., Scher, H. D., Schneider, L., Sluijs, A., Takata, H., Tian, J., Tsujimoto, A., Wade, B. S., Westerhold, T., Wilkens, R. H., Williams, T., Wilson, P. A., Yamamoto, Y., Yamamoto, S., Yamazaki, T., and Zeebe, R. E.: A Cenozoic record of the equatorial Pacific carbonate compensation depth, Nature, 488, 609–614, doi:10.1038/nature11360, 2012.

Payros, A., Ortiz, S., Millán, I., Arostegi, J., Orue-Etxebarria, X., and Apellaniz, E.: Early Eocene climatic optimum: Environmental impact on the north Iberian continental margin, Geol. Soc. Am. Bull., 127, 1632–1644, doi:10.1130/B31278.1, 2015.

Pearson, P. N., van Dongen, B. E., Nicholas, C. J., Pancost, R. D., Schouten, S., Singano, J. M., and Wade, B. S.: Stable warm tropical climate through the Eocene Epoch, Geology, 35, 211–214, 2007.

Perch-Nielsen, K.: Elektronenmikroskopische untersuchungen an Coccolithen und verwandten Formen aus dem Eozan von Danemark, Biologiske Skrifter, Kongelige Danske Videnskabernes Selskab, 18, 1–76, 1971.

Perch-Nielsen, K.: Neue Coccolithen aus dem Maastrichtien von Danemark, Madagaskar und Agypten, B. Geol. Soc. Denmark, 22, 306–333, 1973.

Perch-Nielsen, K.: Cenozoic calcareous nannofossils, in: Plankton stratigraphy, Cambridge Univ. Press, New York, 427–554, 1985.

Pianka, E. R.: On r and K selection, Am. Nat., 104, 592–597, doi:10.1086/282697, 1970.

Premoli Silva, I. and Sliter, W. V.: Cretaceous paleoceanography: Evidence from planktonic foraminiferal evolution, Geol. S. Am. S., 332, 301–328, doi:10.1130/0-8137-2332-9.301, 1999.

Raffi, I. and De Bernardi, B.: Response of calcareous nannofossils to the Paleocene-Eocene Thermal Maximum: Observations on composition, preservation and calcification in sediments from ODP Site 1263 (Walvis Ridge – SW Atlantic), Mar. Micropaleontol., 69, 119–138, doi:10.1016/j.marmicro.2008.07.002, 2008.

Raffi, I., Backman, J., and Pälike, H.: Changes in calcareous nannofossil assemblage across the Paleocene/Eocene transition from the paleo-equatorial Pacific Ocean, Palaeogeogr. Palaeocl., 226, 93–126, doi:10.1016/j.palaeo.2005.05.006, 2005.

Raffi, I., Backman, J., Zachos, J. C., and Sluijs, A.: The response of calcareous nannofossil assemblages to the Paleocene Eocene Thermal Maximum at the Walvis Ridge

in the South Atlantic, Mar. Micropaleontol., 70, 201–212, doi:10.1016/j.marmicro.2008.12.005, 2009.

Riebesell, U., Zondervan, I., Rost, B., Tortell, P. D., Zeebe, R. E., and Morel, F. M. M.: Reduced calcification of marine plankton in response to increased atmospheric CO_2, Nature, 407, 364–367, doi:10.1038/35030078, 2000.

Riebesell, U., Bellerby, R. G. J., Engel, A., Fabry, V. J., Hutchins, D. A., Reusch, K. G., Schulz, T. B. H., and Morel, F. M. M.: Comment on "Phytoplankton calcification in a high-CO_2 world", Science, 322, 1466b, doi:10.1126/science.1161096, 2008.

Romein, A. J. T.: Lineages in early Paleogene calcareous nannoplankton, Utrecht, Micropaleont. Bull., 22, 1–231, 1979.

Rost, B. and Riebesell, U.: Coccolithophores and the biological pump: responses to environmental changes, in: Coccolithophores – From Molecular Processes to Global Impact, Springer, Berlin, 99–125, 2004.

Roth, P. H.: Jurassic and Lower Cretaceous calcareous nannofossils in the western North Atlantic (Site 534): biostratigraphy, preservation, and some observations on biogeography and paleoceanography, DSDP Init. Repts., 76, 587–621, 1983.

Roth, P. H. and Thierstein, H. R.: Calcareous nannoplankton: Leg XIV of the Deep Sea Drilling Project, DSDP Init. Repts., 14, 421–486, 1972.

Schrag, D. P., DePaolo, D. J., and Richter, F. M.: Reconstructing past sea surface temperatures: correcting for diagenesis of bulk marine carbonate, Geochim. Cosmochim. Ac., 59, 2265–2278, 1995.

Scholle, P. A. and Arthur, M. A.: Carbon isotope fluctuations in Cretaceous pelagic limestones: potential stratigraphic and petroleum exploration tool, Am. Assoc. Petr. Geol. B., 64, 67–87, 1980.

Self-Trail, J. M., Powars, D. S., Watkins, D. K., and Wandless, G.: Calcareous nannofossil assemblage changes across the Paleocene-Eocene thermal maximum: Evidence from a shelf setting, Mar. Micropaleontol., 92–93, 61–80, doi:10.1016/j.marmicro.2012.05.003, 2012.

Shackleton, N. J.: Paleogene stable isotope events, Palaeogeogr. Palaeocl., 57, 91–102, 1986.

Shamrai, I. A.: Nekotorye formy verkhnemelovykh i paleogenovykh kokkolitov i diskoasterov na yuge russkol platformy [Certain forms of Upper Cretaceous and Paleogene coccoliths and discoasters from the southern Russian Platform], Izv. Vyssh. Ucheb. Zaved. Geol. i Razv, 6, 27–40, 1963.

Shamrock, J. L.: Eocene calcareous nannofossil biostratigraphy, paleoecology and biochronology of ODP Leg 122 Hole 762c, Eastern Indian Ocean (Exmouth Plateau), PhD thesis, University of Nebraska, 2010.

Slotnick, B. S., Dickens, G. R., Nicolo, M. J., Hollis, C. J., Crampton, J. S., Zachos, J. C., and Sluijs, A.: Large-amplitude variations in carbon cycling and terrestrial weathering during the latest Paleocene and earliest Eocene: The record at Mead Stream, New Zealand, J. Geol., 120, 1–19, doi:10.1086/666743, 2012.

Slotnick, B. S., Lauretano, V., Backman, J., Dickens, G. R., Sluijs, A., and Lourens, L.: Early Paleogene variations in the calcite compensation depth: new constraints using old borehole sediments from across Ninetyeast Ridge, central Indian Ocean, Clim. Past, 11, 473–493, doi:10.5194/cp-11-473-2015, 2015a.

Slotnick, B. S., Dickens, G. R., Hollis, C. J., Crampton, J. S., Strong, C. P., and Phillips, A.: The onset of the Early Eocene Climatic Optimum at Branch Stream, Clarence River

valley, New Zealand, New Zeal. J. Geol. Geop., 58, 262–280, doi:10.1080/00288306.2015.1063514, 2015b.

Spofforth, D. J. A., Agnini, C., Pälike, H., Rio, D., Fornaciari, E., Giusberti, L., Luciani, V., Lanci, L., Muttoni, G., and Bohaty, S. M.: Organic carbon burial following the Middle Eocene Climatic Optimum (MECO) in the central – western Tethys, Paleoceanography, 25, PA3210, doi:10.1029/2009PA001738, 2010.

Stefani, C. and Grandesso, P.: Studio preliminare di due sezioni del Flysch bellunese, Rend. Soc. Geol. It., 14, 157–162, 1991.

Stillman, J. H. and Paganini, A. W., Biogeochemical adaptation to ocean acidifcation, J. Exp. Biol., 218, 1946–1955, doi:10.1242/jeb.115584, 2015.

Stoll, H. M. and Bains, S.: Coccolith Sr / Ca records of productivity during the Paleocene–Eocene thermal maximum from the Weddell Sea, Paleoceanography, 18, 1049, doi:10.1029/2002PA000875, 2003.

Stradner, H.: Die fossilen Discoasteriden Osterreichs, I. Erdöl-Zeitschrift, 74, 178–188, 1958.

Stradner, H.: Vorkommen von Nannofossilien im Mesozoikum und Alttertiär, Erdöl-Zeitschrift für Bohr-und Fördertechnik, 77, 77–88, 1961.

Stradner, H.: New contributions to Mesozoic stratigraphy by means of nannofossils, Proc. Sixth World Petroleum Congress, Section 1 Paper 4, 167–183, 1963.

Sullivan, F. R.: Lower Tertiary nannoplankton from the California Coast Ranges, II, Eocene, University of California Publications in Geological Sciences, 53, 1–74, 1965.

Tagliabue, A. and Bopp, L.: Towards understanding global variability in ocean carbon-13, Global Biogeochem. Cy., 22, GB1035, doi:10.1029/2007GB003037, 2008.

Thibault, N. and Gardin, S.: The calcareous nannofossil response to the end-Cretaceous warm event in the tropical Pacific, Palaeogeogr. Palaeocl., 291, 239–252, doi:10.1016/j.palaeo.2010.02.036, 2010.

Tipple, B. J., Pagani, M., Krishnan, S., Dirghangi, S. S., Galeotti, S., Agnini, C., Giusberti, L., and Rio, D.: Coupled high-resolution marine and terrestrial records of carbon and hydrologic cycles variations during the Paleocene-Eocene Thermal Maximum (PETM), Earth Planet. Sc. Lett., 311, 82–92, doi:10.1016/j.epsl.2011.08.045, 2011.

Toffanin, F., Agnini, C., Fornaciari, E., Rio, D., Giusberti, L., Luciani, V., Spofforth, D. J. A., and Pälike, H.: Changes in calcareous nannofossil assemblages during the Middle Eocene Climatic Optimum: clues from the central-western Tethys (Alano section, NE Italy), Mar. Micropaleontol., 81, 22–31, doi:10.1016/j.marmicro.2011.07.002, 2011.

Toffanin, F., Agnini, C., Rio, D., Acton, G., and Westerhold, T.: Middle Eocene to early Oligocene calcareous nannofossil biostratigraphy at IODP Site U1333 (equatorial Pacific), Micropaleontol., 59, 69–82, 2013.

Tremolada, F. and Bralower, T. J.: Nannofossil assemblage fluctuations during the Paleocene–Eocene Thermal Maximum at Sites 213 (Indian Ocean) and 401 (North Atlantic Ocean): palaeoceanographic implications, Mar. Micropaleontol., 52, 107–116, doi:10.1016/j.marmicro.2004.04.002, 2004.

Vandenberghe, N., Hilgen, F. J., and Speijer, R. P.: The Paleogene Period, in: The Geologic Time Scale 2012, Amsterdam, the Netherlands (Elsevier BV), 855–922, 2012.

Varol, O.: Eocene calcareous nannofossils from Sile (northwest Turkey), Revista Española de Micropaleontología, 21, 273–320, 1989.

Watkins, D. K. and Self-Trail, J. M.: Calcareous nannofossil evidence for the existence of the Gulf Stream during the late Maastrichtian, Paleoceanography, 20, Pa3006, doi:10.1029/2004pa001121, 1992.

Wei, W. and Wise Jr., S. W.: Biogeographic gradients of middle Eocene–Oligocene calcareous nannoplankton in the South Atlantic Ocean, Palaeogeogr. Palaeocl., 79, 29–61, 1990.

Westerhold, T., Röhl, U., Raffi, I., Fornaciari, E., Monechi, S., Reale, V., Bowles, J., and Evans, H. F.: Astronomical calibration of the Paleocene time, Palaeogeogr. Palaeocl., 257, 377–403, doi:10.1016/j.palaeo.2007.09.016, 2008.

Westerhold, T., Röhl, U., Donner, B., McCarren, H. K., and Zachos, J. C.: A complete high – resolution Paleocene benthic stable isotope record for the central Pacific (ODP Site 1209), Paleoceanography, 26, PA2216, doi:10.1029/2010PA002092, 2011.

Winter, A., Jordan, R. W., and Roth, P. H.: Biogeography of living coccolithophores, in: Coccolithophores, edited by: Winter, A. and Siesser, W. G., Cambridge Univ. Press, Cambridge, 161–177, 1994.

Winterer, E. L. and Bosellini, A.: Subsidence and sedimentation on Jurassic passive continental margin, Southern Alps, Italy, Am. Assoc. Petr. Geol. B., 65, 394–421, 1981.

Young, J. R., Geisen, M., and Probert, I.: A review of selected aspects of coccolithophore biology with implications for paleobiodiversity estimation, Micropaleontology, 51, 267–288, 2005.,

Zachos, J. C., Kroon, D., Blum, P., Bowles J., Gaillot, P., Hasegawa, T., Hathorne, E. D., Hodell, D. A., Kelly, D. C., Jung, J.-H., Keller, S. M., Lee Y. S., Leuschner, D. C., Liu, Z., Lohmann, K. C., Lourens, L. J., Monechi, S., Nicolo, M., Raffi, I., Riesselman, C., Röhl, U., Schellenberg, S. A., Schmidt, D., Sluijs, A., Thomas, D., Thomas, E., and Vallius, H.: Early Cenozoic Extreme Climates: The Walvis Ridge Transect, Proc. Ocean Drill. Program, Initial Rep., 208 pp., doi:10.2973/odp.proc.ir.208.2004, 2004.

Zachos, J. C., Röhl, U., Schellenberg, S. A., Sluijs, A., Hodell, D. A., Kelly, D. C., Thomas, E., Nicolo, M., Raffi, I., Lourens, L. J., McCarren, H., and Kroon, D.: Rapid acidification of the ocean during the Paleocene-Eocene Thermal Maximum, Science 308, 1611–1615, doi:10.1126/science.1109004, 2005.

Zachos, J. C., Dickens, G. R., and Zeebe, R. E.: An early Cenozoic perspective on greenhouse warming and carbon-cycle dynamics, Nature, 451, 279–283, doi:10.1038/nature06588, 2008.

Zachos, J. C., McCarren, H., Murphy, B., Röhl, U., and Westerhold, T.: Tempo and scale of late Paleocene and early Eocene carbon isotope cycles: Implications for the origin of hyperthermals, Earth Planet. Sc. Lett., 299, 242–249, doi:10.1016/j.epsl.2010.09.004, 2010.

Zattin, M., Cuman, A., Fantoni, R., Martin, S., Scotti, P., and Stefani, C.: From middle Jurassic heating to Neogene cooling: The thermochronological evolution of the southern Alps, Tectonophysics, 414, 191–202, doi:10.1016/j.tecto.2005.10.020, 2006.

Zeebe, R. E. and Westbroek, P.: A simple model for the $CaCO_3$ saturation state of the ocean: The "Strangelove", the "Neritan", and the "Cretan" ocean, Geochem. Geophy. Geosy., 4, 1104, doi:10.1029/2003GC000538, 2003, 2003.

Zeebe, R. E., Zachos, J. C., and Dickens, G. R.: Carbon dioxide forcing alone insufficient to explain Paleocene-Eocene Thermal Maximum warming, Nat. Geosci., 2, 576–580, doi:10.1038/NGEO578, 2009.

Ziveri, P., Young, J., and van Hinte, J. E.: Coccolithophore export production and accumulation rates, in: On determination of sediment accumulation rates, GeoResearch Forum, Trans Tech Publications LTD, Switzerland, 5, 41–56, 1999.